Oscillatory stimuli differentiate adapting circuit topologies

Sahand Jamal Rahi[1,2], Johannes Larsch[3,4], Kresti Pecani[1], Alexander Y Katsov[3], Nahal Mansouri[5], Krasimira Tsaneva-Atanasova[6], Eduardo D Sontag[7] & Frederick R Cross[1]

Biology emerges from interactions between molecules, which are challenging to elucidate with current techniques. An orthogonal approach is to probe for 'response signatures' that identify specific circuit motifs. For example, bistability, hysteresis, or irreversibility are used to detect positive feedback loops. For adapting systems, such signatures are not known. Only two circuit motifs generate adaptation: negative feedback loops (NFLs) and incoherent feed-forward loops (IFFLs). On the basis of computational testing and mathematical proofs, we propose differential signatures: in response to oscillatory stimulation, NFLs but not IFFLs show refractory–period stabilization (robustness to changes in stimulus duration) or period skipping. Applying this approach to yeast, we identified the circuit dominating cell cycle timing. In *Caenorhabditis elegans* AWA neurons, which are crucial for chemotaxis, we uncovered a Ca^{2+} NFL leading to adaptation that would be difficult to find by other means. These response signatures allow direct access to the outlines of the wiring diagrams of adapting systems.

A complementary approach to elucidating biological systems by traditional molecular biology techniques is to test for response signatures (i.e., characteristic input–output features) that are associated with specific circuit motifs. A confirmed signature establishes the outlines of a biological network before the components are known. The requirements for measuring response signatures are minimal: an experimentally controlled stimulus and a measurable output. Biochemical or genetic manipulations are not inherently necessary. This makes the approach attractive for biological systems that are difficult to manipulate or have many possible genes to pursue. For example, bistability, hysteresis, or irreversibility are signatures of positive feedback loops, and their detection has supported specific mechanisms[1–3].

Adaptation is a dynamic feature of biological systems in which the output returns to (or nears) baseline after stimulation onset. For circuit motifs capable of adaptation, generic response signatures are currently unknown, even though adaptation is ubiquitous and serves important biological functions[4].

Two basic types of circuits can exhibit adaptation: IFFLs and NFLs[5–7] (**Fig. 1a–d**). In adapting pathways, a stimulus *S* (for example, an odor) causes temporary buildup of the response element *R* (for example, intracellular Ca^{2+}), and the subsequent decrease in *R*, which is the hallmark of adaptation, is either independent of *R* (i.e., direct (IFFL)) or dependent on *R* (i.e., indirect, (NFL)). In IFFLs, *S* also generates an inhibitor *I* independently of *R*, and *I* interrupts the buildup of *R* or depletes *R* (**Fig. 1a**). Alternatively, a factor *X*, which contributes to the buildup of *R*, is depleted independently of *R* (**Fig. 1b**). In an NFL, the generation of the inhibitor *I* (or depletion of *X*) depends on *R* itself—i.e., *I* (or *X*) is downstream of *R* (**Fig. 1c**,**d**). The output *O* of the pathway can be *R* or be downstream of *R* (**Fig. 1a–d**). These fundamental options for adaptation (inhibition by *I* or depletion of *X*; dependence on *R* (NFL) or independence (IFFL)) are logically exhaustive, which is supported by computational exploration[6] and rigorous mathematical proofs[7]. Thus, all models describing individual adaptation mechanisms, including integral control[5,8] and state-dependent inactivation[9,10], are subsumed in these two categories; rewriting the models in mathematically equivalent forms can help expose their topologies.

Response signatures for IFFLs and NFLs would help elucidate a wide spectrum of poorly understood biological systems; for example, such measurements ought to resolve contrasting mechanisms that have been proposed for the same system, such as the gonadotropin-releasing hormone pathway[11,12]. The distinction between IFFLs and NFLs is itself biologically important, because each can lead to different system behavior, such as steady state or oscillations[13].

[1]Laboratory of Cell Cycle Genetics, The Rockefeller University, New York, New York, USA. [2]Center for Studies in Physics and Biology, The Rockefeller University, New York, New York, USA. [3]Howard Hughes Medical Institute, Lulu and Anthony Wang Laboratory of Neural Circuits and Behavior, The Rockefeller University, New York, New York, USA. [4]Department of Genes–Circuits–Behavior, Max Planck Institute of Neurobiology, Martinsried, Germany. [5]Division of Pulmonary and Critical Care Medicine, Brigham and Women's Hospital, Boston, Massachusetts, USA. [6]Department of Mathematics, College of Engineering, Mathematics and Physical Sciences and EPSRC Centre for Predictive Modelling in Healthcare, University of Exeter, Exeter, UK. [7]Department of Mathematics and Center for Quantitative Biology, Rutgers, The State University of New Jersey, Piscataway, New Jersey, USA. Correspondence should be addressed to S.J.R. (sjrahi@rockefeller.edu).

RECEIVED 4 DECEMBER 2016; ACCEPTED 24 JULY 2017; PUBLISHED ONLINE 28 AUGUST 2017; DOI:10.1038/NMETH.4408

Dynamical stimuli have been used to explore biological pathways[14] and to uncover interesting biology[15–18]. Specifically, step-like and ramp-like inputs have been applied to distinguish specific models[8,19–23]. In an attempt to explore the general applicability of these approaches, we simulated simple adapting models and found various counterexamples, which show that it is at least unclear how previous discriminants can be used generally (**Supplementary Fig. 1a–h**). And varying stimulus strengths (ramps, for example) can be problematic: many inducible promoters are 'all or nothing' and thus threshold the stimuli. Furthermore, at different concentrations or strengths, stimuli may activate different subnetworks[24], confounding the analysis.

RESULTS

We found that a single on–off stimulus pulse does not suffice for discrimination of adapting circuit types, as IFFL and NFL models fit the same experimental adaptation time course equally well (**Supplementary Fig. 1i,j**).

Refractory period stabilization

The next, more complicated on–off stimulation pattern consists of two or more pulses. Considering two simple representations of IFFLs and NFLs (**Fig. 1e,f** and **Supplementary Fig. 1k,l**), we noticed a fundamental difference in their responses to a second stimulus pulse. In an IFFL, the inhibitor I grows (or X decreases) independently of the response (up to saturation) (**Fig. 1a,b**); therefore, the longer the first stimulus pulse is, the smaller the response to a second stimulus pulse should be (**Fig. 1e**). With NFLs (**Fig. 1f**), in contrast, if the first stimulus is long enough for adaptation to 'kick in', the entire circuit can be effectively shut off, and the inhibition mechanism (I or X) can begin to reset; further lengthening the first stimulus pulse matters little for the second response (**Fig. 1f**). So the recovery time or the 'refractory period' should always be increasing with the stimulus duration in IFFLs and should be stabilized (robust) in NFLs.

We needed a general, rigorous definition for the refractory period and thus considered repeated on–off stimuli of duration d and period T; we defined the refractory period $T_{max}(d)$ as the period at which the time-averaged output $<O(t,d,T)> =: O(d,T)$ is maximal for fixed d (**Fig. 1g,h**). At $T_{max}(d)$, the stimuli produce maximal output. This generalizes the common understanding of the refractory period, where for T below T_{max}, stimulus pulses are too fast for the system to recover due to adaptation ($O(d, T)$ decreases with decreasing $T < T_{max}$), and above T_{max}, the responses recover, but their time average decreases ($O(d, T) \sim 1/T$ for $T >> T_{max}$).

For the IFFL and NFL models in **Figure 1e,f**, we calculated $T_{max}(d)$ analytically and found that the slope of $T_{max}(d)$ is > 1 everywhere for the IFFL model, while the NFL model's $T_{max}(d)$ is flat (slope = 0) for intermediate d (**Fig. 1i,j**), which describes refractory period stabilization quantitatively. To check more complicated models numerically, we set 1/2 as a practical threshold for the slope $\partial T_{max}/\partial d$, between the minimum slopes in **Figure 1i,j**. We consider the refractory period 'stabilized' if its slope is below 1/2 in an appropriate range of pulse durations d (to be determined by numerical exploration; see below).

There are a number of inherent advantages to defining the refractory period by periodic stimuli and the maximum of the time-averaged output (**Supplementary Note 1**), including for the mathematical analysis and for the experimental data analysis. Crucially, this paradigm allows us to explicitly analyze only the refractory periods of small circuits; the same results hold ($T_{max}(d)$ is invariant) for an infinite number of additions to these circuits (**Fig. 1k** and **Supplementary Note 1**).

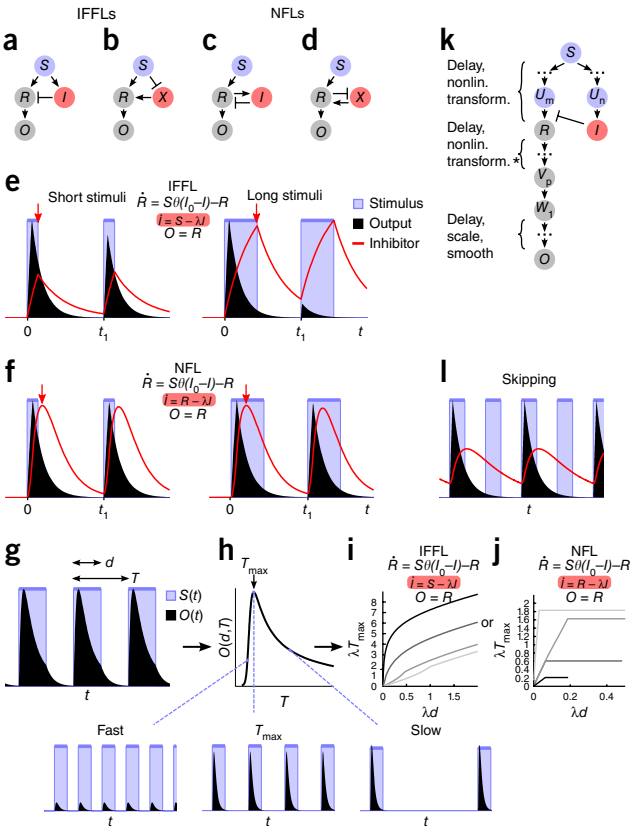

Figure 1 | Discriminating IFFLs and NFLs. (**a–d**) Four fundamental wiring diagrams for adaptation. Arrows can represent multiple intermediate nodes. (**e**,**f**) IFFL (**e**) or NFL (**f**) system receiving two consecutive stimulus pulses of different widths but with the same onset times. Stimuli always turn on at times 0 and t_1. Red arrows indicate when the I begins to decay. (**g**) Periodic stimulus pulses of duration d and period T produce output $O(t) = O(t, d, T)$. (**h**) $O(d, T)$ has a maximum at $T_{max}(d)$. Periodic solutions shown for stimuli that are faster (left), equal to (middle), or slower (right) than T_{max}. (**i**) IFFL model as in **e** (IFFL 1 in **Supplementary Fig. 2** with $n \to \infty$). Model parameters: $\lambda I_0 = 0.01, 0.1, 0.5, 0.75$ (dark to light). (**j**) NFL model as in **f** (NFL 1 in **Supplementary Fig. 2** with $n \to \infty$). NFL parameters: $(\lambda, \lambda I_0) = (0.1,0.3), (0.1,0.1), (0.4,0.1), (0.1,0.01)$ (dark to light). $T_{max}(d)$ plot terminates when d exceeds the absolute refractory time, above which the circuit would be activated twice for each stimulus pulse. $\theta(x)$, step function (0 for $x < 0$ and 1 otherwise). (**k**) Schematic showing equivalent classes of circuits with the same $T_{max}(d)$. The asterisk denotes the specific nature of the nonlinear transformations (nonlin. transform.) analyzed (see **Supplementary Note 1**). (**l**) Period skipping in an NFL circuit. Levels of stimulus, inhibitor, and output are shown in arbitrary units as a function of time (**e–g**,**h**,**l**).

Period skipping

Another response signature can be deduced by considering that when an NFL adapts to a stimulus, the entire circuit can be shut off from the stimulus until the inhibition resets and the system recovers (**Fig. 1l**). Any stimuli administered while the circuit is insulated ought to have little effect. This would result in responses

Table 1 | Period skipping and refractory period stabilization are generic in NFLs but not in IFFLs

Circuit type	Total tested	Adapting	Skipping and refractory period stabilization
NFL	315,549	22,188	9,712 (44%)
IFFL	307,584	16,502	48 (0.29%)
Ratio			150:1

These results are based on a computational analysis of the set of circuit models in **Supplementary Figures 2–6**.

'skipping' stimulus pulses (a simple response pattern might be 0-1-0-1-0… (**Fig. 1l**), although more complicated patterns are possible (**Supplementary Fig. 1m**,**n**)).

IFFLs cannot exhibit such dynamics because of the following properties (**Supplementary Note 2**).

(1) Period skipping cannot occur in purely feed-forward systems (such as the IFFLs modeled in this work including **Fig. 1e**,**i**) because these systems entrain to the stimulus period *T*.

(2) Adding positive feedback loops (PFLs) to a (purely feed-forward) IFFL does not produce period skipping, because a PFL system of two species cannot show period skipping.

(3) General PFL systems cannot access period skipping solutions with on–off stimuli.

These results rule out period skipping in biologically realistic IFFL circuits, leaving that possibility generically to NFLs.

Generality and uniqueness of discriminants

To explore how generic or unique these response signatures are (uniqueness of period skipping in NFLs is guaranteed), we systematically analyzed nonlinear IFFL and NFL models numerically. (We had to go beyond linear models, as they entrain and their $O(d, T)$ are monotonic.)

First, we ruled out that the observed differences between IFFLs and NFLs were particular to the abrupt nature of the inhibition function or to the output functions in **Figure 1i**,**j**. We replaced the step function $\theta(I_0 - I)$ by Michaelis–Menten terms with Hill coefficients ≥1 and varied parameters and output functions (**Supplementary Table 1**). None of the IFFL models showed refractory period stabilization or period skipping, whereas 71% of the NFL models, which showed sufficient adaptation (Online Methods), did. Thus, the two NFL signatures were robust to such variations.

For a more comprehensive exploration of model space, we generated $>6 \times 10^5$ implementations of IFFLs and NFLs with 86 differing wiring diagrams, interaction types, and numbers of nodes. Specifically, we analyzed systems with (i) inhibitors *I* or activators *X* (**Fig. 1a**–**d**), (ii) inhibitors that block the increase of a target or degrade the target, (iii) nonzero baseline activities, (iv) saturation due to Michaelis–Menten kinetics, (v) nonlinearities due to cooperativity, and (vi) additional dynamical nodes (**Supplementary Figs. 2**–**6**). We varied parameters in an unbiased manner (0.1, 1, 10 for most parameters). We focused particularly on finding false positives (IFFL loops showing refractory period buffering) rather than minimizing false negatives (NFL loops failing to show signatures), which underestimates the generality of period skipping in NFLs (Online Methods). For the same reason, we limited ourselves to 4 subtypes of NFLs with 3 + 1 nodes (+1 for output node) but covered all 82 possible IFFLs with 3 + 1 or 4 + 1 nodes. As expected, none of the IFFL circuits showed period skipping.

A small number of IFFL circuits showed refractory period stabilization when the stimulus duration (*d*) was small, where our previous argument based on intermediate *d* values (**Fig. 1e**,**f**) does not apply. Requiring that refractory period stabilization occurs when *d* is large enough (1.5× adaptation time), left few false positives, and the likelihood of assigning an NFL circuit correctly would be 150:1 (**Table 1** and **Supplementary Fig. 7**).

We were surprised to find that both signatures occurred with or without cooperativity. Also, refractory period stabilization was detected about as often as period skipping in our computational searches (0.8:1; **Table 1** and data not shown), suggesting that neither is rare.

Published models

We also analyzed two classes of models from the literature that are thought to describe a wide spectrum of biological systems (**Supplementary Note 3**). The state-dependent inactivation model[9,10], which is essentially an IFFL, showed neither period skipping nor refractory period stabilization, as expected. Fold-change detection models[25] can be either IFFLs or NFLs. Using previously published models[26], we detected period skipping in the NFLs but neither NFL signature in the IFFLs, as expected.

Application to experimental systems

To demonstrate the experimental application of our findings, we began with trial runs to establish the pulse widths and periods appropriate for the biological system at hand. We chose the smallest and largest appropriate pulse durations to find T_{max} at those durations. We reasoned that by the mean value theorem, determining the slope of a straight line through two data points is sufficient to infer the slope of any smooth interpolation at a point in between, which shows refractory period stabilization. In that process, we also detected period skipping around the smallest pulse periods we applied, which an analysis of the simple NFL models in **Figure 1f**,**j** suggested (**Supplementary Fig. 8**).

Circuits dominating cell cycle timing in *S. cerevisiae*

The cell cycle control system in budding yeast involves dozens of interacting genes and consists at its core of at least the CDK–APC/C oscillator[27] (**Fig. 2a**–**f**) and a proposed 'global transcriptional oscillator' (GTO)[28–31], a cyclical chain of transcription factors (**Fig. 2g**). Given the many different subsystems, it is unclear which ones, if any, predominantly set cell cycle dynamics.

We deleted the genes encoding cyclins Cln1, Cln2, and Cln3 and introduced a construct (*MET-CLN2*) expressing start cyclin Cln2 during methionine withdrawal (–Met) to place cell cycle start under exogenous control, resulting in *cln1-3Δ MET-CLN2* (*clnΔ**) cells[32] and eliminating the PFL and the early NFL 1 (**Fig. 2b**,**d**,**h**–**k**). With a long –Met pulse activating *MET-CLN2*, which stops short of initiating a second cell cycle, transcription of cell cycle periodic genes rises and falls once[32], demonstrating that the system adapts to Cln2, which rules out the simplest version of the GTO lacking IFFLs or NFLs. We also introduced a *CLN2* promoter–driven *YFP* construct (*CLN2pr-YFP)* to report start (SBF) cluster gene activity, which turns on roughly with budding (**Fig. 2h**).

We administered five –Met (Cln2 on) pulses of varying durations *d* and periods *T* (**Fig. 2i**,**j**). For long periods, cells responded to all five pulses (≈60% (n = 102) at d = 50 min, T = 65 min)

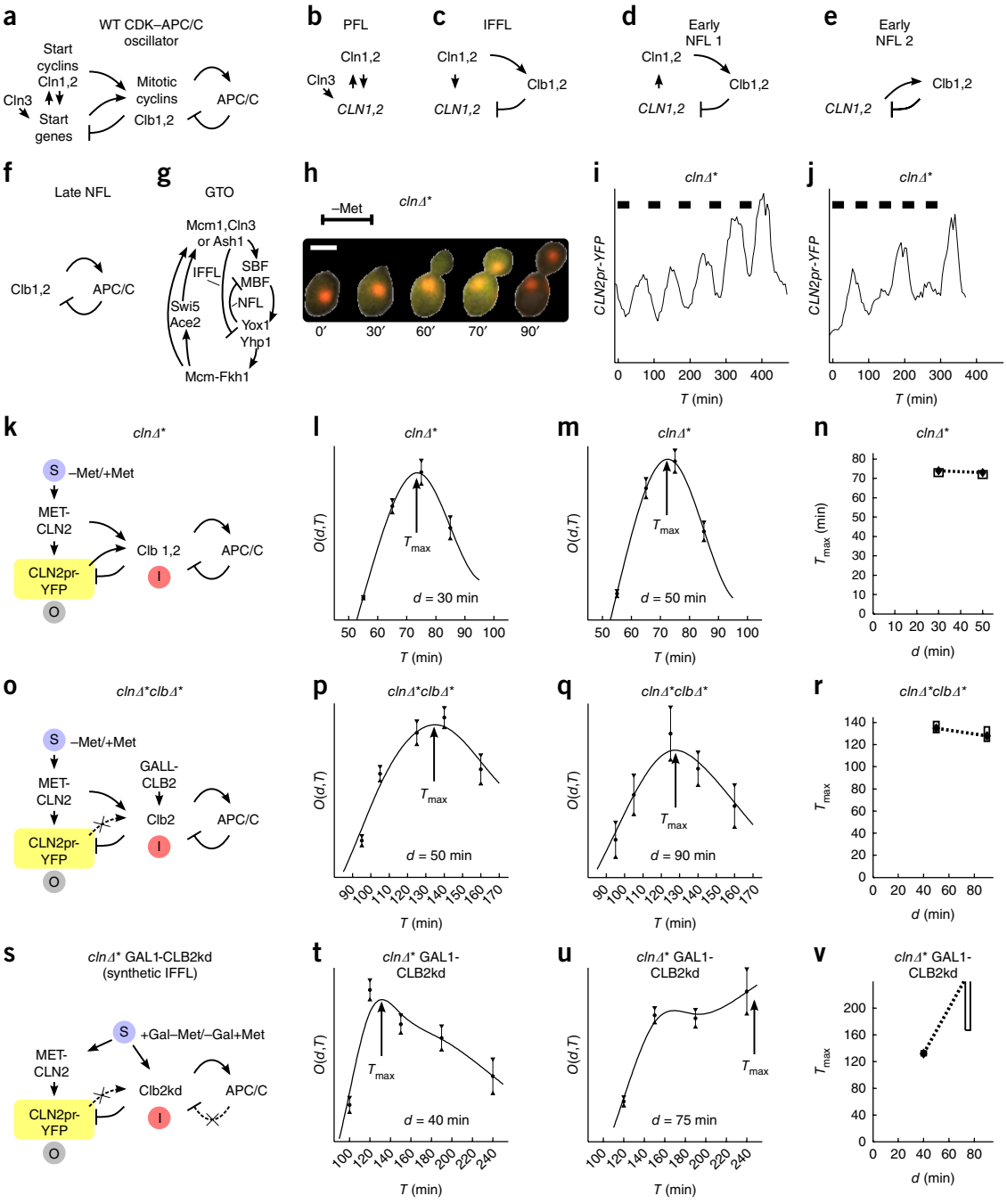

Figure 2 | Signatures identify dynamically important NFLs in yeast cell cycle control mutants and can be abolished by an artificial IFFL. (**a**) Schematic of the wild-type CDK–APC/C cell cycle control system. (**b**–**f**) Subcircuits from **a**. Black arrows summarize multiple nodes and interactions[27]. (**g**) Schematic of GTO model (adapted from refs. 30,31). (**h**) A *clnΔ** cell undergoes one cell cycle after *MET-CLN2* is induced from 0 to 30 min in –Met medium. Nuclei are marked by Htb2-mCherry. Scale bar, 5 μm. (**i**) Sample time course of *CLN2pr-YFP* in a *clnΔ** cell subjected to 5 –Met pulses of d = 30 min and period T = 85 min (black bars), inducing five complete cell cycles. (**j**) A *clnΔ** cell showing period skipping (–Met pulses d = 30 min, T = 65 min (black bars)). The cell cycle starts (and completes) only in response to pulses 1, 3, 5, as determined by budding, nuclear division, and cytokinesis. (**k**–**v**) Schematic of CDK-APC/C cell cycle control system in indicated strains (**k**,**o**,**s**). Crossed-out, dashed arrows indicate circuits and interactions that have been eliminated or disrupted. Output (fluorescence from fraction of consistently responding cells) mean ± s.e.m. vs. stimulus period T for fixed d, shown together with smooth spline fit used for estimating the peaks (**l**,**m**,**p**,**q**,**t**,**u**). The numbers of cells (about 100–200) underlying each data point are specified in Online Methods. Best fit $T_{max}(d)$ (diamond), central 90% confidence interval (box), and linear interpolation (dashed line) (**n**,**r**,**v**). Vertical axes (**i**,**j**,**l**,**m**,**p**,**q**,**t**,**u**) have arbitrary units. All cells express the *CLN2pr-YFP* construct.

(**Fig. 2i**). In contrast, with short periods, cells commonly skipped stimulus pulses (14% (n = 126) performed 5 cell cycles with d = 50 min, T = 55 min) (**Fig. 2j**). Given our mathematical results, we concluded that the overall dynamic was governed by NFLs; for example, early NFL 2, late NFL, or the GTO NFLs (**Fig. 2e**–**g**). IFFLs (**Fig. 2c**,**g**) had a minor role, if any. Skipping of forced cell cycles was observed previously in a different genetic context[33].

In the cell cycle system, the refractory period describes the time it takes for the cell cycle to reset and is potentially correlated with cell cycle completion. It is not known which subcircuits, if any, make this timing robust. We defined the output $O(d, T)$ as the fraction of consistently responding (non-skipping) cells, multiplied by their *CLN2pr-YFP* signal (Online Methods and **Supplementary Fig. 9**). The peak in $O(d, T)$, defining the refractory period, was due to fast pulses lowering the fraction of cells that responded to *MET-CLN2* pulses and large periods decreasing the time-averaged *CLN2pr-YFP* signal. T_{max} was remarkably stable (73–74 min, ≈ cell cycle period for mother cells in synthetic complete (SC) medium and glucose) as we changed d (30 min, 50 min) (**Fig. 2l**–**n**, slope $T_{max}(d) < 1/2$ with >99.9% confidence). Thus, in addition to period skipping, refractory period stabilization also indicated that cell cycle dynamics was set by NFLs, not IFFLs.

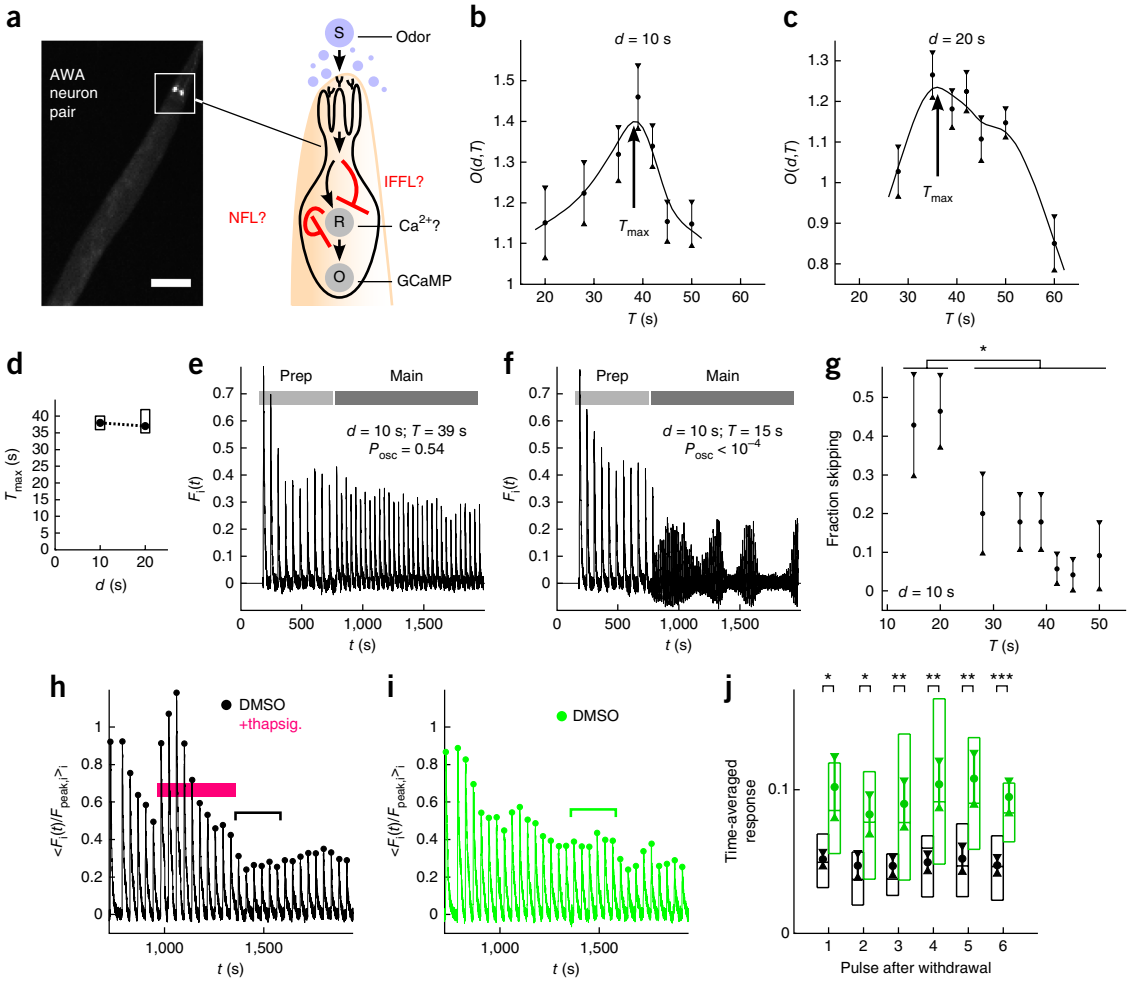

Figure 3 | A Ca^{2+}-NFL leads to adaptation in *C. elegans* AWA neurons. (**a**) *C. elegans* worms expressing GCaMP2.2b in the AWA olfactory sensory neurons pulsed with diacetyl. The question mark indicates that the detailed molecular mechanism of Ca^{2+} adaptation, including circuit type and the adapting node R, were unknown. Scale bar, 100 µm. (**b**,**c**) Output mean ± s.e.m. vs. stimulus period T for fixed pulse duration d, shown together with smooth spline fit used for estimating the peaks. Number of worms underlying each data point (left to right) 28 ,15, 28, 28, 35, 24, 11 (**b**), 29, 49, 62, 37, 31, 27, 11 (**c**). (**d**) Mean $T_{max}(d)$ (circle), central 90% confidence interval (box), and linear interpolation (dashed line). For d = 10 s, mean = 38 s, interval = 36–40 s; for d = 20 s, mean = 37 s, interval = 35–42 s. (**e**,**f**) Recordings without (**e**) or with (**f**) detectable period skipping at intermediate (T = 39 s) or small (T = 15 s) stimulus periods, respectively. The first 10 preparatory pulses have the same period and duration across all trials. (**g**) Fraction of worms ± s.e.m. showing significant period skipping (P_{osc}< 0.05, Online Methods) at d = 10 s. *, differences between fractions are at least significant with respect to the one-tailed P = 0.05 threshold. (**h**,**i**) Ca^{2+} levels before, during, and after thapsigargin (**h**) or DMSO (**i**) application. The first pulse shown was the last preparatory pulse. For the remaining pulses, d = 20 s, T = 39 s. Data are normalized by the average of the last two prep response pulse peak heights (Online Methods). Medium contains 0.3% DMSO throughout. Data are mean over 25 (**h**) or 13 (**i**) worms. (**j**) Time average of the response pulses after removal of thapsigargin in **h** (black), compared to control in **i** (green), showing continued depression of the responses. Circle, mean; triangles, s.e.m.; box boundaries, interquartile range; center line, median. Pulses analyzed are indicated by black or green brackets in **h** or **i**, respectively. *P < 0.05, **P < 0.01, ***P < 0.001 (one-sided), difference of means.

We wondered whether refractory period robustness was a consequence of the interlocking NFLs in the system (**Fig. 2a**,**k**). We therefore deleted cyclin genes *CLB1–CLB6*, resulting in *clnΔ*clb1-6Δ GALL-CLB2* (*clnΔ*clbΔ**) cells, and induced mitotic cyclin Clb2 constitutively in these cells in galactose. This eliminated the early NFL 2 (**Fig. 2e**) as well as any transcriptional control of mitotic cyclins (**Fig. 2o**). Again, the refractory period turned out to be well stabilized (128–135 min, ≈ cell cycle period in SC galactose) when d (50 min or 90 min) changed (**Fig. 2p–r**, slope $T_{max}(d) < 1/2$ with >98% confidence). Thus, the early NFL 2, in addition to the early NFL 1 and the IFFLs, is unnecessary for normal overall timing and robustness in the cell cycle control system, at least in galactose.

To investigate whether the late NFL (**Fig. 2f**) between B-type cyclins and APC was responsible for refractory period stabilization, we constructed a *clnΔ* GAL1-CLB2kd* strain, in which a pulse of galactose and –Met simultaneously induces cell cycle entry, transcription start, and a pulse of undegradable Clb2kd, which blocks mitotic exit[34,35]. After long waiting periods, these cells completed the cell cycle, probably owing to autonomous pulses of the Cdc14 phosphatase that ultimately overcomes Clb2kd inhibition[35]. This system constitutes an artificial IFFL (**Fig. 2s**). Here $T_{max}(d)$ changed markedly between 132 min at d = 40 min and >167 min at d = 75 min (**Fig. 2t–v**, slope $T_{max}(d) > 1/2$ with >99.9% confidence). This was due to longer Clb2kd induction blocking transcription start for longer periods, as expected for an IFFL (**Fig. 1e**). Thus, this artificial IFFL revealed the predicted $T_{max}(d)$ signature for IFFLs. Therefore, our procedure was effective at detecting IFFLs. Furthermore, breaking or overriding all three CDK-APC/C NFLs, including the late Clb1–Clb2–CDK–APC/C loop, eliminated refractory period stabilization. The late Clb1–Clb2–CDK–APC/C NFL dominated the dynamics. The other circuits, including the GTO adaptation loops, had a minor role in the overall cell cycle dynamics.

Circuit for adaptation in *C. elegans* AWA neurons

Response adaptation is a core feature of most neurons and has a key role in behavior[4]. We turned to sensory neurons in *C. elegans*, several of which, such as AWA, ADL, and ASH, show a spike and subsequent adaptation in intracellular Ca^{2+} upon step-like odor stimulation. Ca^{2+} adaptation, specifically, is thought to have a key role in *C. elegans* behavior[24,36]. We focused on the AWA neuron pair, which is one of two main chemoattractive olfactory sensory neuron pairs in *C. elegans*[37]. Although many genes involved in *C. elegans* sensory processing have been discovered, molecular circuit-level understanding of adaptation, a key neuronal computation, is currently lacking.

We analyzed odor-evoked Ca^{2+} responses in intact, wild-type worms (**Fig. 3a**). We stimulated worms expressing an AWA-specific Ca^{2+} sensor (GCaMP2.2b)[24,38] with periodic on–off pulses of diacetyl, an odor known to activate AWA[38] (**Supplementary Fig. 10a–g**). For stable responses and for calibration purposes, we first administered a series of ten preparatory odor pulses[24,38]. We then measured total AWA Ca^{2+} output for seven different pulse periods T at two pulse durations (10 s and 20 s) (**Fig. 3b–e**). The output peaked at refractory period T_{max} = 37–38 s at both pulse durations (**Fig. 3b–d**); thus, the slope of $T_{max}(d)$ was close to 0 in between (<1/2 with confidence 0.96) and was therefore stabilized, indicating an NFL.

Also, with fast odor pulses (T = 15 or 20 s), many of the worms showed clearly noticeable period skipping (**Fig. 3f**). We devised a statistical test (P_{osc}) for detecting low-frequency modulations[32] (Online Methods) and observed a significant increase in the number of worms with low-frequency response modulations in recordings at T = 15 or 20 s, compared to other periods (**Fig. 3g**). According to our mathematical analysis, this was another indicator of an NFL.

We wondered whether Ca^{2+} forms an NFL onto itself. In the absence of our measurements, we had no particular reason to pursue this hypothesis given that previous results, if anything, suggested an IFFL[39,40]. We tested for a Ca^{2+} NFL in AWA by dynamically manipulating Ca^{2+} levels using thapsigargin, a widely used inhibitor of SERCA pumps, which remove Ca^{2+} from the cytosol[41]. We added thapsigargin to the medium for ten odor pulses (**Fig. 3h**). Odor-induced Ca^{2+} responses surged initially, as expected for thapsigargin. However, the responses adapted again within 5–7 odor pulses, consistent with Ca^{2+} boosting its own inhibition mechanism. Removal of thapsigargin caused a depression of Ca^{2+} levels (hyper-adaptation) compared to the no-drug control (**Fig. 3i**,**j**), which is consistent with the inhibition mechanism decaying slowly, reflecting a memory of elevated Ca^{2+} levels. In contrast, elevated Ca^{2+} would not increase inhibition in an IFFL, and after thapsigargin removal, odor responses would be at normal levels. Subsequent recovery showed that over-adaptation was not due to (permanent) damage. Furthermore, longer thapsigargin treatment excluded Ca^{2+} depletion or nonspecific cell exhaustion as the cause of adaptation (**Supplementary Fig. 10h**). Thapsigargin itself did not act noticeably as an odor (**Supplementary Fig. 10i**). As the changes in Ca^{2+} were at biologically relevant timescales and magnitudes, these results provide evidence for a physiological Ca^{2+} NFL causing adaptation in AWA neurons in intact *C. elegans*.

DISCUSSION

The refractory period is a natural way of characterizing adapting systems, in part because it involves quantities with intuitive units (time, for d and T_{max}; none for $\partial T_{max}/\partial d$). It is also germane to biology and not derived from other fields of science or engineering.

Our approach has inherent limitations: not all IFFLs and NFLs can be distinguished by dynamical measurements[42], and the detection of circuit motifs does not, for example, specify biochemical species. However, our response signatures were reliable and useful in practice, and the same limitations apply to bistability, hysteresis, and irreversibility, which do not identify all PFLs[43] but are nevertheless useful. Furthermore, multiple motifs may exist in the same biological system; however, we expect and found that one circuit is dominant at a specific timescale.

A stabilized refractory period implies that NFLs have robust timing, which may confer advantages such as rendering cell cycle timing robust to noise. We speculate that this leads to the predominance of NFLs in nature, which may also be why the dependence of the refractory period on stimulus duration, a generic property of IFFLs, has been overlooked. Skipping in NFLs represents a strong high-frequency filter that ignores fast pulses. For the cell cycle this may be advantageous, but for other systems, the failure to track inputs might represent a trade-off in exchange for other NFL properties, such as a stable refractory period.

METHODS

Methods, including statements of data availability and any associated accession codes and references, are available in the online version of the paper.

Note: Any Supplementary Information and Source Data files are available in the online version of the paper.

ACKNOWLEDGMENTS

We thank C.I. Bargmann for mentorship, support, and comments on the manuscript. We thank E. Siggia for fruitful discussions. The work was supported by US National Institutes of Health grant 5RO1-GM078153-07 (F.R.C.), NRSA Training Grant CA009673-36A1 (S.J.R.), a Merck Postdoctoral Fellowship at The Rockefeller University (S.J.R.), and the Simons Foundation (S.J.R.). J.L. was supported by a fellowship from the Boehringer Ingelheim Fonds. E.D.S. was partially supported by the US Office of Naval Research (ONR N00014-13-1-0074) and the US Air Force Office of Scientific Research (AFOSR FA9550-14-1-0060).

AUTHOR CONTRIBUTIONS

Conceptualization and writing: S.J.R., J.L., K.P., A.Y.K., N.M., K.T.-A., E.S., and F.R.C. Experiments and data analysis: S.J.R., J.L., and K.P. Mathematical proofs: S.J.R. and E.D.S.

COMPETING FINANCIAL INTERESTS

The authors declare no competing financial interests.

1. Pomerening, J.R., Sontag, E.D. & Ferrell, J.E. Jr. Building a cell cycle oscillator: hysteresis and bistability in the activation of Cdc2. *Nat. Cell Biol.* **5**, 346–351 (2003).
2. Xiong, W. & Ferrell, J.E. Jr. A positive-feedback-based bistable 'memory module' that governs a cell fate decision. *Nature* **426**, 460–465 (2003).
3. Charvin, G., Oikonomou, C., Siggia, E.D. & Cross, F.R. Origin of irreversibility of cell cycle start in budding yeast. *PLoS Biol.* **8**, e1000284 (2010).
4. Alberts, B. *et al. Molecular Biology of the Cell* (Garland Science, 2015).
5. Behar, M., Hao, N., Dohlman, H.G. & Elston, T.C. Mathematical and computational analysis of adaptation via feedback inhibition in signal transduction pathways. *Biophys. J.* **93**, 806–821 (2007).
6. Ma, W., Trusina, A., El-Samad, H., Lim, W.A. & Tang, C. Defining network topologies that can achieve biochemical adaptation. *Cell* **138**, 760–773 (2009).
7. Ascensao, J.A. *et al.* Non-monotonic response to monotonic stimulus: Regulation of glyoxylate shunt gene-expression dynamics in Mycobacterium tuberculosis. *PLOS Comput. Biol.* **12**, e1004741 (2016).
8. Alon, U. *An Introduction to Systems Biology* (Chapman and Hall/CRC, 2007).
9. Friedlander, T. & Brenner, N. Adaptive response by state-dependent inactivation. *Proc. Natl. Acad. Sci. USA* **106**, 22558–22563 (2009).
10. Ferrell, J.E. Jr. Perfect and near-perfect adaptation in cell signaling. *Cell Syst.* **2**, 62–67 (2016).
11. Lim, S. *et al.* Negative feedback governs gonadotrope frequency-decoding of gonadotropin releasing hormone pulse-frequency. *PLoS One* **4**, e7244 (2009).
12. Tsaneva-Atanasova, K., Mina, P., Caunt, C.J., Armstrong, S.P. & McArdle, C.A. Decoding GnRH neurohormone pulse frequency by convergent signalling modules. *J. R. Soc. Interface* **9**, 170–182 (2012).
13. Tyson, J.J., Chen, K.C. & Novak, B. Sniffers, buzzers, toggles and blinkers: dynamics of regulatory and signaling pathways in the cell. *Curr. Opin. Cell Biol.* **15**, 221–231 (2003).
14. Castillo-Hair, S.M., Igoshin, O.A. & Tabor, J.J. How to train your microbe: methods for dynamically characterizing gene networks. *Curr. Opin. Microbiol.* **24**, 113–123 (2015).
15. Segall, J.E., Block, S.M. & Berg, H.C. Temporal comparisons in bacterial chemotaxis. *Proc. Natl. Acad. Sci. USA* **83**, 8987–8991 (1986).
16. Geva-Zatorsky, N., Dekel, E., Batchelor, E., Lahav, G. & Alon, U. Fourier analysis and systems identification of the p53 feedback loop. *Proc. Natl. Acad. Sci. USA* **107**, 13550–13555 (2010).
17. Mitchell, A., Wei, P. & Lim, W.A. Oscillatory stress stimulation uncovers an Achilles' heel of the yeast MAPK signaling network. *Science* **350**, 1379–1383 (2015).
18. Heltberg, M., Kellogg, R.A., Krishna, S., Tay, S. & Jensen, M.H. Noise induces hopping between NF-κB entrainment modes. *Cell Syst.* **3**, 532–539.e3 (2016).
19. Block, S.M., Segall, J.E. & Berg, H.C. Adaptation kinetics in bacterial chemotaxis. *J. Bacteriol.* **154**, 312–323 (1983).
20. Tu, Y., Shimizu, T.S. & Berg, H.C. Modeling the chemotactic response of *Escherichia coli* to time-varying stimuli. *Proc. Natl. Acad. Sci. USA* **105**, 14855–14860 (2008).
21. Muzzey, D., Gómez-Uribe, C.A., Mettetal, J.T. & van Oudenaarden, A. A systems-level analysis of perfect adaptation in yeast osmoregulation. *Cell* **138**, 160–171 (2009).
22. Wang, C.J., Bergmann, A., Lin, B., Kim, K. & Levchenko, A. Diverse sensitivity thresholds in dynamic signaling responses by social amoebae. *Sci. Signal.* **5**, ra17 (2012).
23. Takeda, K. *et al.* Incoherent feedforward control governs adaptation of activated ras in a eukaryotic chemotaxis pathway. *Sci. Signal.* **5**, ra2 (2012).
24. Larsch, J. *et al.* A circuit for gradient climbing in *C. elegans* chemotaxis. *Cell Rep.* **12**, 1748–1760 (2015).
25. Shoval, O. *et al.* Fold-change detection and scalar symmetry of sensory input fields. *Proc. Natl. Acad. Sci. USA* **107**, 15995–16000 (2010).
26. Adler, M., Szekely, P., Mayo, A. & Alon, U. Optimal regulatory circuit topologies for fold-change detection. *Cell Syst.* **4**, 171–181.e8 (2017).
27. Morgan, D.O. *The Cell Cycle: Principles of Control* (New Science Press, 2007).
28. Simon, I. *et al.* Serial regulation of transcriptional regulators in the yeast cell cycle. *Cell* **106**, 697–708 (2001).
29. Lee, T.I. *et al.* Transcriptional regulatory networks in *Saccharomyces cerevisiae*. *Science* **298**, 799–804 (2002).
30. Orlando, D.A. *et al.* Global control of cell-cycle transcription by coupled CDK and network oscillators. *Nature* **453**, 944–947 (2008).
31. Simmons Kovacs, L.A. *et al.* Cyclin-dependent kinases are regulators and effectors of oscillations driven by a transcription factor network. *Mol. Cell* **45**, 669–679 (2012).
32. Rahi, S.J., Pecani, K., Ondracka, A., Oikonomou, C. & Cross, F.R. The CDK-APC/C oscillator predominantly entrains periodic cell-cycle transcription. *Cell* **165**, 475–487 (2016).
33. Charvin, G., Cross, F.R. & Siggia, E.D. Forced periodic expression of G1 cyclins phase-locks the budding yeast cell cycle. *Proc. Natl. Acad. Sci. USA* **106**, 6632–6637 (2009).
34. Wäsch, R. & Cross, F.R. APC-dependent proteolysis of the mitotic cyclin Clb2 is essential for mitotic exit. *Nature* **418**, 556–562 (2002).
35. Drapkin, B.J., Lu, Y., Procko, A.L., Timney, B.L. & Cross, F.R. Analysis of the mitotic exit control system using locked levels of stable mitotic cyclin. *Mol. Syst. Biol.* **5**, 328 (2009).
36. Hilliard, M.A. *et al.* In vivo imaging of *C. elegans* ASH neurons: cellular response and adaptation to chemical repellents. *EMBO J.* **24**, 63–72 (2005).
37. Rengarajan, S. & Hallem, E.A. Olfactory circuits and behaviors of nematodes. *Curr. Opin. Neurobiol.* **41**, 136–148 (2016).
38. Larsch, J., Ventimiglia, D., Bargmann, C.I. & Albrecht, D.R. High-throughput imaging of neuronal activity in *Caenorhabditis elegans*. *Proc. Natl. Acad. Sci. USA* **110**, E4266–E4273 (2013).
39. Colbert, H.A. & Bargmann, C.I. Odorant-specific adaptation pathways generate olfactory plasticity in *C. elegans*. *Neuron* **14**, 803–812 (1995).
40. Kato, S., Xu, Y., Cho, C.E., Abbott, L.F. & Bargmann, C.I. Temporal responses of *C. elegans* chemosensory neurons are preserved in behavioral dynamics. *Neuron* **81**, 616–628 (2014).
41. Zwaal, R.R. *et al.* The sarco-endoplasmic reticulum Ca^{2+} ATPase is required for development and muscle function in *Caenorhabditis elegans*. *J. Biol. Chem.* **276**, 43557–43563 (2001).
42. Shoval, O., Alon, U. & Sontag, E. Symmetry invariance for adapting biological systems. *SIAM J. Appl. Dyn. Syst.* **10**, 857–886 (2011).
43. Ferrell, J.E. Jr. Self-perpetuating states in signal transduction: positive feedback, double-negative feedback and bistability. *Curr. Opin. Cell Biol.* **14**, 140–148 (2002).

ONLINE METHODS

Computational exploration of model circuits. The following algorithm was implemented in MATLAB R2010b.

1. Ordinary differential equations (ODEs) with parameters and interactions described in **Supplementary Figures 2–6** and **Supplementary Table 1** were generated.

2. Steady-state levels were calculated for the dynamic variables at $S = 0$ and $S = 1$ (only $S = 0$ for NFLs) by plugging the model parameters into formulas for the steady-state solutions, which had been derived for each model by hand. If the steady-state levels were not defined (i.e., $\pm\infty$), the model was not analyzed further.

3. To quantify how well the model adapted, the ODEs were solved numerically for a step stimulus ($S = 0$ to $S = 1$). Nine output nonlinearities ($O = R$, $O = R^2$, $O = R^3$, …) corresponding to the output functions in **Supplementary Figures 2–6** and **Supplementary Table 1** were tested. Only those models and output functions were pursued further, in which adaptation was sufficiently strong (after a transient peak, the output declined by more than 80%).

4. The ODEs were then solved with repeated on ($S = 1$) and off ($S = 0$) stimuli of duration d and period T using MATLAB's ode45 function. We employed various means to speed up the calculations, such as interpolating initial conditions based on neighboring solutions and extrapolating exponential convergence. The computations were stopped if the solution vector $\mathbf{x}(t)$ converged $||\mathbf{x}(t_i)-\mathbf{x}(t_i-T)||/||\mathbf{x}(t_i)|| < 10^{-12}$, where t_i is the time point right after the i'th $S = 1$ stimulus, before $20{,}000/T$ repetitions. If the solutions did not converge, a test for period skipping was performed and, if positive, the model was counted toward the number of adapting models in **Table 1** and **Supplementary Table 1**, but otherwise not analyzed further. For period skipping, the solutions to the last $n = \{1,\ldots,5\}$ stimulus pulses were simply checked for convergence to the n prior solutions (fractional error $< 10^{-12}$). We focused particularly on finding false positives (IFFL loops showing refractory period buffering) rather than minimizing false negatives (NFL loops failing to show signatures) by gearing our computer code primarily to calculating $T_{max}(d)$ and detecting period skipping only if it occurs in that process. Since the search algorithm stopped when period skipping was detected, the number of models with period skipping includes models which may also stabilize refractory periods.

5. Initially, a fixed set of pulse durations $d = \{0.05, 0.15\ldots0.55, 0.75\ldots2.15, 2.65\}$ and a set of periods T ranging from $d + 0.005$ to 10 or 30 (depending on d) were studied. If $O(d, T)$ was increasing for the largest values of T in this set, T was increased incrementally (up to a maximum value of 1,000) until $O(d, T)$ decreased. If $O(d, T)$ had a maximum as a function of T, the intervals around the maximum were bisected to identify the maximum more accurately. If $O(d, T)$ had multiple maxima as a function of T, the largest period corresponding to a maximum was taken for $T_{max}(d)$. Only those models were pursued further, in which $O(d, T)$ showed a maximum for $T > d$, i.e., where $T_{max} > d$, for some d in the initial set. The number of these models was added to the number of adapting models from step 4, and the sums are indicated in **Table 1** and **Supplementary Table 1**. Thus, we counted as the number of adapting models those that adapted sufficiently to a step function and showed either a nontrivial T_{max} refractory period or period skipping.

6. If $O(d, T)$ had a maximum for $T > d$ for any of the initial d values (step 5), d was increased and $T_{max}(d)$ calculated until the slope of $T_{max}(d)$ ($\partial T_{max}(d)/\partial d$) approached 1 or until T_{max} exceeded the maximum allowed T. Then, $T_{max}(d)$ was smoothed everywhere by calculating additional $T_{max}(d)$ points on a denser set of d where the slope of $T_{max}(d)$ changed rapidly.

***S. cerevisiae* strains.** All strains were W303 congenic. Strains SJR14a4d and SJR12a5a were used previously[32]. The *CLB2kd* mutation and the *GAL1-CLB2kd* construct have been described[34,35] and were crossed into SJR14a4d to yield SJR82c10b. Genotypes were as follows: SJR14a4d, *cln1Δ cln2Δ:CLN2pr-Venus:TRP1 cln3Δ:LEU2 trp1Δ:TRP1:MET3-CLN2 HTB2-mCherry:HIS5*; SJR12a5a, SJR14a4d background, *clb1Δ-clb6Δ:KanMX clb2Δ:GALL-CLB2:URA3-clb5Δ:KanMX clb3Δ:TRP1 clb4Δ:his3:KanMX*; SJR82c10b, SJR14a4d background, *ura3Δ:GAL1-CLB2kd:URA3*.

***C. elegans* strains.** We used the N2-based CX14887 strain with integrated *gpa-6::GCaMP2.2b* (ref. 24). Animals were raised at 20 °C on nematode growth medium (NGM) plates seeded with *Escherichia coli* OP50 bacteria as a food source. All experiments were performed with young adults, age synchronized by picking larval stage 4 (L4) animals to fresh food plates 12–24 h before the experiment.

Experimental setup. For *S. cerevisiae* experiments, cells were grown overnight and diluted to $OD_{660} \approx 0.02$ about 6 h before the experiment to ensure return to log phase. Fluorescence microscopy was performed on cells trapped in a microfluidic device (CellASIC) while the medium was changed. Initially, cells were synchronized by arresting in off ($S = 0$) medium for 120 min. Then, the medium was switched periodically between on ($S = 1$) and off ($S = 0$) pulse medium. SC medium was supplemented as follows: SJR14a4d overnight medium, glucose, no methionine (D–Met); on pulse medium, D–Met; off pulse medium, glucose + methionine (D+Met); SJR12a5a overnight medium, galactose (G), no methionine (G–Met); on pulse medium, G–Met; off pulse medium, G+Met; SJR82c10b overnight medium, raffinose (R)–Met; on pulse medium, R+G–Met; off pulse medium, R+Met. Images were taken every 5 min.

For *C. elegans* experiments, the experimental setup was basically as described[38] for paralyzed worms. In all pulsing experiments, we switched between S basal medium with 1 mM (−)-tetrasimole hydrochloride (Sigma-Aldrich) with (odor on) or without (odor off) 1.15 μM diacetyl (Sigma-Aldrich).

The time interval between images was 0.1 s. In every experiment, 10 preparatory odor pulses were administered (10 s duration, 60 s period) before switching to the main measurement pulses of duration d and period T. (The eleventh pulse followed 60 s after the beginning of the tenth pulse.)

For the thapsigargin experiments, we dissolved the drug (Santa Cruz Biotech) at 10 mg/ml in DMSO and then dissolved the solution at 0.3% by volume in S basal. The final concentration of thapsigargin was about 46 μM. We spun the thapsigargin–S basal solution down in microcentrifuge tubes at 13,200 r.p.m. for 1 min and saw no precipitation. For the DMSO-only controls, we added DMSO at 0.3% by volume to S basal.

Image and data analysis for *S. cerevisiae* experiments. Automated image segmentation and fluorescence quantification of yeast grown under time-lapse conditions were performed as previously described[3]. To find $T_{max}(d)$ for each yeast mutant, we needed to measure the time-averaged output $O(d, T)$ for fixed pulse duration d as the pulse period T was varied. In brief, we defined the system output $O(d, T)$ as the fraction of cells $p(d, T)$ that underwent normal cell cycles at least until some time point t, multiplied by their time-averaged *CLN2pr-YFP* fluorescence $y(d, T)$ just before t. We estimated $T_{max}(d)$ by fitting a spline through the means of the $O(d, T)$ data points, and calculated the uncertainty on the basis of the standard errors in $O(d, T)$. All times are relative to the onset of the first stimulus pulse at 0 min.

In all experiments, we applied 5 on–off pulses, which allowed us to follow and quantify about 100–200 cells for each d and T. More than 5 pulses generally led to overgrowth in the imaging arena, as each stimulus pulse roughly doubled the number of cells. The exact number of cells analyzed for each data point were as follows (left to right): 201, 136, 194, 125 (**Fig. 2l**); 126, 102, 100, 70 (**Fig. 2m**); 130, 150, 123, 174, 67 (**Fig. 2p**); 110, 123, 97, 162, 62 (**Fig. 2q**); 69, 273, 287, 129, 61 (**Fig. 2t**); 389, 346, 212, 95 (**Fig. 2u**). The number of cells was determined by the noise in each data point; additional cell colonies were analyzed when the s.e.m. was too large compared to the mean to allow a reasonable comparison with other data points.

To define and compare the output $O(d, T)$ for different T, we needed a specific, fixed time point t in our recordings that was late enough that a sufficient number of pulses had been administered but that would also occur in all of the recordings with the same strain. With the number of pulses fixed, the experiments with shorter periods are overall shorter. We chose the onset of the last stimulus pulse $t = 4\ T_2$ of the second-shortest stimulus period T_2 for each strain ($T_2 = 65$ min for *clnΔ**, $T_2 = 105$ min for *clnΔ*clbΔ**, $T_2 = 120$ min for *clnΔ* GAL1-CLB2kd*) because it was a late time point, contained in all related recordings, and allowed the following quantification: We counted the number of cells $n(d, T)$ that replicated in response to every stimulus pulse before t and at least budded in response to the first stimulus pulse starting after t, if any. These cells skipped no stimulus pulses at least until t and the following stimulus pulse. For example, cells pulsed with period T_2 had to undergo four normal, on-time cell cycles and at least bud a fifth time to be counted. Cells pulsed with period $2T_2$ had to undergo two normal, on-time cell cycles and at least bud in response to the third stimulus pulse. The ratio of these cells compared to the initial number of cells $N(d, t)$ defined $p(d, T) = n(d, T)/N(d, T)$, and the standard error was $\Delta P = (P(1 - P) / N)^{1/2}$, where $P = (n + 2) / (N + 4)$ takes into account the Agresti–Coull correction. We suppress the dependence on d and T, i.e., $P = P(d, T)$, when the notation becomes too cumbersome otherwise. The *CLN2pr-YFP* fluorescence time courses of these (non-skipping) cells ($F_i(t)$) were averaged ($\langle F_i(t)\rangle_i$) and the height of the first peak in $\langle F_i(t)\rangle_i$ was computed (F_{norm}) to normalize each recording. F_{norm} was obviously independent of T. The running average of $F_i(t)/F_{norm}$ was computed over a time window of size T (average from $t - T/2$ to $t + T/2$ assigned to t). The running average was again averaged from $3T_2$ to $3.5T_2$ for the *clnΔ** and *clnΔ*clbΔ** experiments and from $2T_2$ to $3T_2$ for the *clnΔ* GAL1-CLB2kd* experiment to yield y_i. Using these running averages ensured that mostly only fluorescence measurements from before t were taken into consideration, which ensures that these cells are not skipping and performing on time and normal cell cycles. The mean (y) and standard error (Δy) of all y_i values were computed.

The mean of the output was defined as $O(d, T) = p(d, T)y(d, T)$ with standard error $\Delta O(d, T) = [\Delta p(d, T)^2 y(d, T)^2 + p(d, T)^2 \Delta y(d, T)^2]^{1/2}$, where we neglected the small $\Delta p(d, T)^2 \Delta y(d, t)^2$ term. We approximated the distribution of $O(d, T)$ by a Gaussian with s.d. $\Delta O(d, T)$ and generated 10^4 random configurations of different outputs at each T. Using MATLAB, we fit smoothing splines through each one of the configurations. The maximum of the spline was taken as the T_{max} for each sampled configuration. The whole distributions of $T_{max}(d)$ generated for the two pulse durations d for each strain were compared to each other. The confidence values for refractory period stabilization that we report are the fraction of T_{max} slopes smaller than 0.5. We varied the smoothing parameter for the smoothing spline over a wide range (0.001, 0.01, 0.1, 0.3) but the confidences for the slope of $T_{max}(d)$ hardly changed. For the plots, we used smoothing parameters 0.1, 0.01, 0.001 for *clnΔ**, *clnΔ*clbΔ**, *clnΔ* GAL1-CLB2kd*, respectively, reflecting the different distances between data points in T.

Image and data analysis for *C. elegans* experiments. *Tracking AWA neurons*. The images were processed basically as described[38]. Occasionally, the worms moved despite general paralysis due to tetramisole in the medium. To determine the coordinates of the AWA neurons in time, we tracked GCaMP2.2b fluorescence in each frame computationally (residual fluorescence, sufficient to identify AWA, was detectable even when the odor was off); the previously described NeuroTracker software suite (ref. 38) was used (**Supplementary Fig. 10a**). We tried to track the AWA neurons of every worm in the arena, for which, in some instances, repeated manual readjustments of the brightness threshold to identify the AWA neurons were necessary. We gave up tracking individual worms if the AWA detection could not be stabilized despite repeated manual interventions. This was the case for about 1 in 15 worms in each experiment, where, usually, another close-by worm interfered with and diverted the tracker.

Background and baseline subtraction. For each worm i, the average raw intensity $F_{R,i}(t)$ was read out of a 13 × 13 pixel square window (4 μm/pixel) centered on the tracked AWA neurons' coordinates (**Supplementary Fig. 10a**). In order to correct for background, the median intensity $F_{BG,i}(t)$ in a ring around worm i's AWA neurons (ring inner radius, 10 pixels; outer radius, 19 pixels) was also read out and subtracted to yield $F_{noBG,i}(t) = F_{R,i}(t) - F_{BG,i}(t)$ (**Supplementary Fig. 10b**).

Next, we corrected for baseline fluorescence, which can drift during the course of the recordings; so, we constructed a time-dependent baseline function (**Supplementary Fig. 10c**). Here and elsewhere, we used a 5–second time window from −7.5 seconds to −2.5 seconds before odor pulses reached the microfluidic chamber to define the baseline fluorescence preceding each odor pulse, and we defined the center of the window (at −5 s) as the beginning of each output pulse. We calculated the average of $F_{noBG,i}(t)$ over each such time window preceding each odor pulse. A piecewise linear function $F_{BL,i}(t)$ was fit through these baseline averages, which were assigned to the beginning of each odor pulse. Between these points, $F_{BL,i}(t)$ interpolated linearly. Thus, $F_{BL,i}(t)$ reflected shifts in the baseline fluorescence in time. Using

doi:10.1038/nmeth.4408

this time-dependent baseline function, we normalized the signal, $F_i(t) = (F_{noBG,i}(t) - F_{BL,i}(t)) / F_{BL,i}(t)$ (**Supplementary Fig. 10d**).

Exclusion of poorly responding worms. We tried to record and compute the responses of every worm in our experiments, but we excluded 10% of the worms from further analysis because their responses were obviously problematic. To filter worms in an objective fashion, we set up quantitative criteria. We applied these tests to $F_{noBG,i}(t)$, that is, after background correction but before baseline correction (**Supplementary Fig. 10b**). The first 10 preparatory odor pulses (of 10 s duration and 60 s period), which preceded the main measurement pulses in every experiment, allowed the worms to be evaluated before and independently of their responses to the main odor pulses and in a consistent manner across all experiments. The responses to prep pulses 9 and 10 were especially important because we used them to calibrate the rest of the responses.

We filtered out worms whose output pulses 9 and 10 varied too much from one another; we eliminated 8 (of 463 total) worms because the baseline $F_{BL,i}(t)$ changed by more than 6% before and after pulse 9 (or before and after pulse 10) with respect to the average of $F_{BL,i}(t)$ before and after pulse 9 (or 10). (Exclusion if $|F_{BL,i}(t_j) - F_{BL,i}(t_{j+1})| / (F_{BL,i}(t_j) / 2 + F_{BL,i}(t_{j+1}) / 2) > 0.06$, where t_j is the start of pulse j, and j is either 9 or 10 (**Supplementary Fig. 10b**).)

Of the remaining, we filtered out 40 worms because the signal-to-noise ratio was too low; we defined the signal-to-noise ratio as the height of pulse 9 or 10 divided by the s.d. of the baseline ($F_{noBG,i}(t)$ over the preceding 5-s time window) before or after pulses 9 or 10. (Exclusion if $\sigma(F_{noBG,i}(t))_{t = \{tj-2.5'',\ldots,tj+2.5''\}} / (F_{noBG,i}(t_k) - F_{BL,i}(t_j)) > 0.11$ for at least two of the four possible combinations where t_j is the start of pulse 9, 10, or 11, and t_k is the time of the peak of the closest output pulse 9 or 10.) One such trace is plotted in orange in **Supplementary Figure 10b**.

These thresholds are, of course, ultimately arbitrary, however, we think the criteria were reasonable, as (i) they were used in a consistent manner across all experiments; (ii) we applied them to preparatory pulses before and independently of the responses to the main odor pulses; (iii) we only excluded the 'worst' 10% of all of the worms in our experiments; (iv) we included all of the worms that we could track initially, for example, despite weak AWA responses; and (v) all of the response traces that were discarded were visibly problematic and unusual.

Calculation of average responses. For the worms that passed the two filters, we calculated $F_{norm,i}$, the average of $F_i(t)$ over the responses to pulses 9 and 10, i.e., over a time window starting at the beginning of odor pulse 9 and extending to the start of odor pulse 11. $F_{norm,i}$ serves to normalize the AWA responses for each worm (**Supplementary Fig. 10e**). Again, odor pulses 9 and 10 are the last prep pulses; beginning with pulse 11, we switched to odor pulse duration d and period T. Next, we computed the running average of $F_i(t)$ from pulse 11 onward over a time window of size T (**Supplementary Fig. 10e**). We normalized the running average of each worm by $F_{norm,i}$ (**Supplementary Fig. 10f**). We fit a linear least-squares regression through the normalized running average, starting 100 s after the start of odor pulse 11 and ending 700 s thereafter (**Supplementary Fig. 10f**). For T = 39 s pulses, about three full odor pulses had been administered (2 × 39 s + 10 s or 2 × 39 s + 20 s) before the start of the linear fit. The span of 700 s is fairly long (about 18 × 39 s period pulses, for example) and it allowed us to include all of our recordings, including some experiments that aborted early. For each worm, we took as the output $O_i(d, T)$ the estimated response at 100 s by calculating the value of the linear fit at 100 s (**Supplementary Fig. 10g**). The mean and the s.e.m. over $O_i(d, T)$ are shown in **Figure 3** and **Supplementary Figure 10g**. Taking points later than 100 s from the same linear fit as the output $O_i(d, T)$ yielded similar results: the confidence that the slope of T_{max} between d = 10 s and d = 20 s is less than 0.5 is 0.96 at 100 s, 0.96 at 200 s, 0.94 at 300 s, 0.87 at 400 min. The gradual loss of confidence at later times can be due to experimental artifacts, accumulation of random noise with time, loss of correlation to the prep pulses, or, potentially, the activation of pathways with slower time scales, and so on. As shown in **Supplementary Figure 9a**, it is important to compare the output at a specific time after the onset of stimulation. Given the high confidence of our results up to about 300 s after the onset of the main odor pulses, we did not investigate these issues further.

Similarly to the *S. cerevisiae* measurements, we repeated experiments for a particular pulse period width d and period T with about 15 worms per experiment until the s.e.m./mean ratio appeared small enough by visual comparison with the neighboring data points. Upon completion of the experiments we performed our statistical analyses, which were unambiguous, and thus we did not go back for more measurements.

Calculation of T_{max}, slopes, and confidence intervals. Based on the mean and s.e.m. of the output $O_i(d, T)$ over all worms i for each T for any fixed d, we approximated the distribution by a Gaussian and generated 10^4 random configurations of different outputs at each T. Using MATLAB, we fit a smoothing spline with smoothing parameter 0.1 through each one of the configurations. With noticeably smoother (smoothing parameter, 0.01; resulting confidence, 0.94) or more flexible (smoothing parameter, 0.3; resulting confidence, 0.96) splines, we arrived at essentially the same results (confidences in the slope of T_{max}). The maximum of the spline was taken as the T_{max} for each configuration. The whole distribution of T_{max} thus generated for pulse duration d = 10 s was compared to the distribution of T_{max} for pulse duration d = 20 s. The confidence values for refractory period stabilization that we report are the fraction of T_{max} slopes smaller than 0.5.

Statistical test for period skipping. The test for period skipping used here was developed from a related statistical oscillation test[32]. The basic idea is to (i) find the best fit of an enveloping sinusoidal function of period $T' > T$ for each recording, and (ii) compare the goodness of the fit to best fits for random reshufflings of the same recording. The fraction of random reshufflings that produce better fits than the original recording defines P_{osc}. Specifically, for each recording, we calculated Fourier-type coefficients $c_i(T') = \Sigma'_t F_i(t)\, e^{i2\pi t/T'}$, where the Σ'_t only includes time points t beginning with the first odor pulse at least 100 s after the beginning of odor pulse 11. As described above, ignoring the first 100 s of the main odor responses served as a rough way to allow some of the initial transients to dissipate. $c(T')$ was calculated for skipping periods T' ranging from 0 s to 600 s by 1-s increments. The largest possible skipping period 600 s was chosen so as to allow at least two full skipping periods to fit into most of our recordings. As the best fit, we chose the largest $|c(T')|^2$ peak after the peak at $T' = T$. Then, we created 10^3 reshufflings of the original recording by cutting up

each recording in intervals of length T beginning with the first odor pulse after 100 s after the beginning of pulse 11 and permuting them. For each reshuffled recording we computed the largest $|c(T')|^2$, as before. We finally ranked the largest $|c(T')|^2$ for the original recording against the reshuffled data to obtain P_{osc}. Because there is no noise in the numerical analysis of circuit models, and because we were willing to accept false negatives (missing period skipping in some NFLs) for faster computations, the periodicity test that we applied in our computational search of model space was much simpler.

Comparison of thapsigargin to control. To compare responses of worms that were treated with thapsigargin versus DMSO-only controls, we averaged the traces in each group and normalization by the average of the last two prep response pulse peak heights for **Figure 3h–j**. (Normalization by the mean of the last two prep response pulses yielded similar results.)

Data availability. The data that support the findings of this study are available from the corresponding author upon reasonable request. A **Life Sciences Reporting Summary** for this paper is available.

Code availability. The code used for computational exploration of model circuits is available as **Supplementary Software**.

doi:10.1038/nmeth.4408

nature research

Corresponding author(s): Sahand Jamal Rahi

☐ Initial submission ☐ Revised version ☒ Final submission

Life Sciences Reporting Summary

Nature Research wishes to improve the reproducibility of the work that we publish. This form is intended for publication with all accepted life science papers and provides structure for consistency and transparency in reporting. Every life science submission will use this form; some list items might not apply to an individual manuscript, but all fields must be completed for clarity.

For further information on the points included in this form, see Reporting Life Sciences Research. For further information on Nature Research policies, including our data availability policy, see Authors & Referees and the Editorial Policy Checklist.

Experimental design

1. Sample size

Describe how sample size was determined.

We recorded and analyzed yeast cells and worms about 30 or 15 at a time, respectively. We continued repeating experiments with more cells or worms for a specific stimulation period and width until the means and standard errors appeared sufficiently clear compared to those of neighboring data points visually. When we performed our mathematical analyses, the statistics were sufficiently unambiguous so that we did not have to go back and record more.

2. Data exclusions

Describe any data exclusions.

We excluded 10% of the worms, which responded worst BEFORE the onset of the pulsing experiments. The reasons were responses that fluctuated too strongly or low signal-to-noise ratios, both assessed before the main measurement. See Methods for details.

3. Replication

Describe whether the experimental findings were reliably reproduced.

We pooled the results of multiple repeated measurements, i.e., repeated measurements of about 30 yeast cells or about 15 worms for each stimulation period and width.

4. Randomization

Describe how samples/organisms/participants were allocated into experimental groups.

Groups were defined solely by genotypes and pulsing patterns (pulse period and width).

5. Blinding

Describe whether the investigators were blinded to group allocation during data collection and/or analysis.

Unbiased, computational analysis of data.

Note: all studies involving animals and/or human research participants must disclose whether blinding and randomization were used.

Nature Methods: doi:10.1038/nmeth.4408

6. Statistical parameters

For all figures and tables that use statistical methods, confirm that the following items are present in relevant figure legends (or in the Methods section if additional space is needed).

n/a	Confirmed
☐	☒ The exact sample size (*n*) for each experimental group/condition, given as a discrete number and unit of measurement (animals, litters, cultures, etc.)
☐	☒ A description of how samples were collected, noting whether measurements were taken from distinct samples or whether the same sample was measured repeatedly
☐	☒ A statement indicating how many times each experiment was replicated
☐	☒ The statistical test(s) used and whether they are one- or two-sided (note: only common tests should be described solely by name; more complex techniques should be described in the Methods section)
☐	☒ A description of any assumptions or corrections, such as an adjustment for multiple comparisons
☐	☒ The test results (e.g. *P* values) given as exact values whenever possible and with confidence intervals noted
☐	☒ A clear description of statistics including central tendency (e.g. median, mean) and variation (e.g. standard deviation, interquartile range)
☐	☒ Clearly defined error bars

See the web collection on statistics for biologists for further resources and guidance.

Software

Policy information about availability of computer code

7. Software

Describe the software used to analyze the data in this study.	Image analysis software previously published and referenced. Code for exploration of model space described in detail in Methods section and supplied.

For manuscripts utilizing custom algorithms or software that are central to the paper but not yet described in the published literature, software must be made available to editors and reviewers upon request. We strongly encourage code deposition in a community repository (e.g. GitHub). *Nature Methods* guidance for providing algorithms and software for publication provides further information on this topic.

Materials and reagents

Policy information about availability of materials

8. Materials availability

Indicate whether there are restrictions on availability of unique materials or if these materials are only available for distribution by a for-profit company.	No unique materials were used.

9. Antibodies

Describe the antibodies used and how they were validated for use in the system under study (i.e. assay and species).	No antibodies used.

10. Eukaryotic cell lines

a. State the source of each eukaryotic cell line used.	No mammalian cell lines were used. See Methods for yeast strains.
b. Describe the method of cell line authentication used.	No mammalian cell lines were used. See Methods for yeast strains.
c. Report whether the cell lines were tested for mycoplasma contamination.	*Confirm that all cell lines tested negative for mycoplasma contamination OR describe the results of the testing for mycoplasma contamination OR declare that the cell lines were not tested for mycoplasma contamination OR state that no eukaryotic cell lines were used.*
d. If any of the cell lines used are listed in the database of commonly misidentified cell lines maintained by ICLAC, provide a scientific rationale for their use.	*Provide a rationale for the use of commonly misidentified cell lines OR state that no commonly misidentified cell lines were used.*

Nature Methods: doi:10.1038/nmeth.4408

Animals and human research participants

Policy information about studies involving animals; when reporting animal research, follow the ARRIVE guidelines

11. Description of research animals

Provide details on animals and/or animal-derived materials used in the study.	N2-based CX14887 C. elegans was used.

Policy information about studies involving human research participants

12. Description of human research participants

Describe the covariate-relevant population characteristics of the human research participants.	No human research participants were used.

Nature Methods: doi:10.1038/nmeth.4408

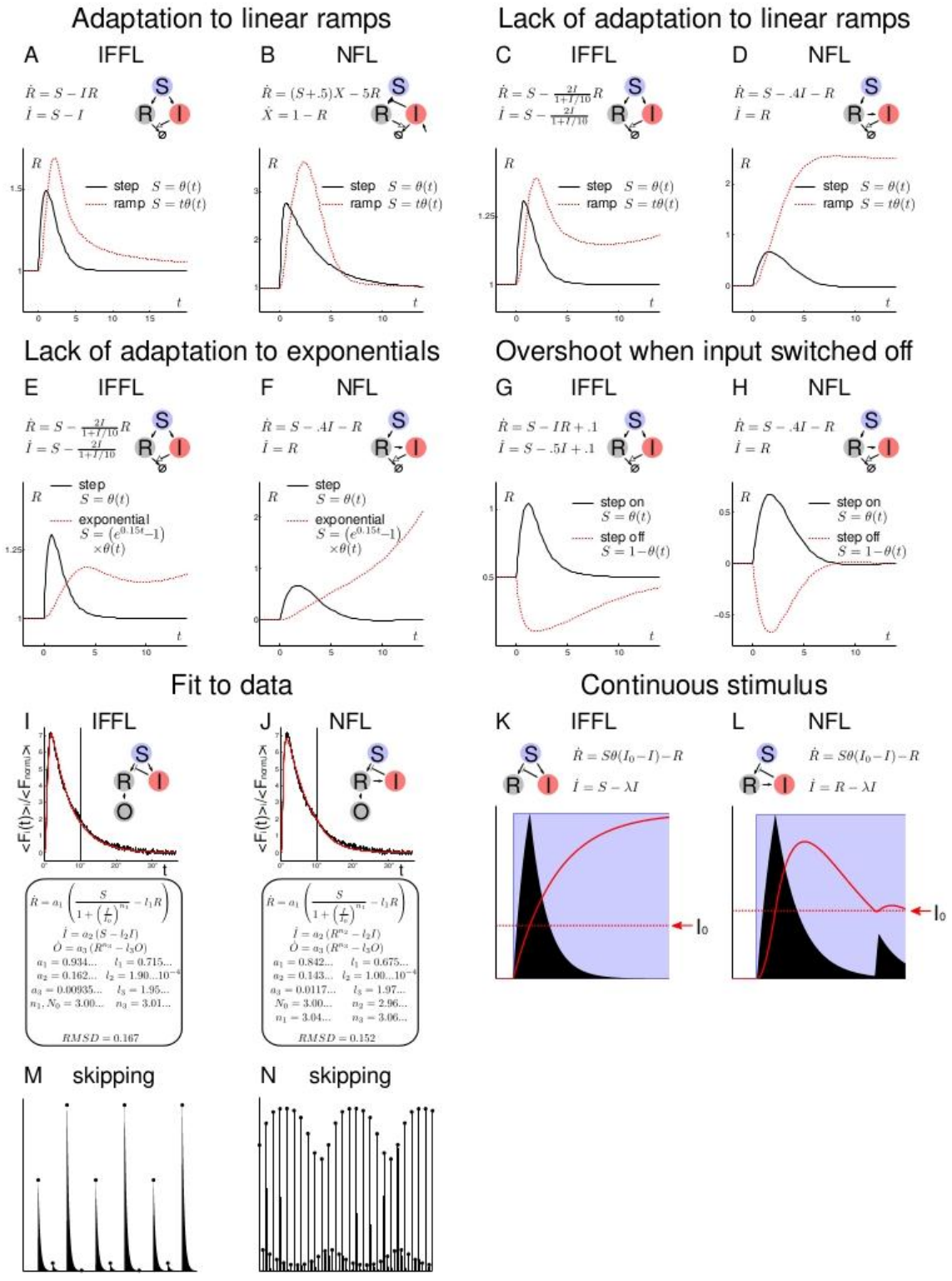

Supplementary Figure 1

Examples showing that IFFLs and NFLs can show qualitatively similar responses to linearly ramping, exponentially ramping, or on-off stimuli; fits to the same experimental data; model circuits under continuous stimulation; and examples of period skipping for NFLs.

A-H: Examples showing that various response characteristics from the literature can appear in both IFFLs and NFLs. Adapted from refs.(8,19-23) $\theta(t)$ is a step function, which is zero for $t < 0$ and equal to one for $t > 0$. The linear ramp $t\theta(t)$ is equal to t for $t > 0$ and equal to zero for $t < 0$. The exponential ramp $(e^{xt} - 1)\times\theta(t)$ is equal to $(e^{xt} - 1)$ for $t > 0$ and equal to zero for $t < 0$. A, B: Adaptation to step inputs and linear ramps; C, D: adaptation to step inputs but failure to adapt to linear ramps; E, F: adaptation to step inputs but failure to adapt to exponential ramps; G, H: overshoot below steady-state when the input is turned off (red dashed line, switch $S = 1$ to $S = 0$ at $t = 0$). I, J: Fits to the same experimental data: Black: The 15'th response pulses at odor pulse duration $d = 10''$ and period $T = 42''$ were taken from our C. elegans recordings, averaged over all worms, and then normalized to the mean of the 9'th and 10'th response pulses. Red: We guessed parameters for each model and then fine-tuned them to the data by a steepest-descent algorithm minimizing the root mean square deviation (RMSD). K, L: Examples showing the behavior of the circuits in Fig. 1 E, F (same as Fig. 1 I, J) under continuous stimulation. With long stimulus (S) pulses (blue), the response R is effectively shut off from the stimulus S when I exceeds I_0 in the model circuits in Fig. 1 E, F (same as Fig. 1 I, J). In the NFL circuit, I can drop below I_0 again while the stimulus is on, allowing the stimulus S to cause another spike in R, and repeat. However, softening the step inhibition function (here: $\theta(I_0 - I)$) easily abolishes sustained oscillations (not shown). For the model calculations in Fig. 1 J, we plot $T_{max}(d)$ for pulse durations d before there is a second response spike elicited by the same stimulus pulse. M, N: Examples of period skipping with 4T-periodic (M, one NFL) or more complicated (N, interlocking NFLs) responses to T-periodic stimuli. Peaks are marked by black circles. Periodic stimuli are not shown. K-N: Levels of Stimulus, Inhibitor, and Output (color-coded) indicated in arbitrary units as a function of time.

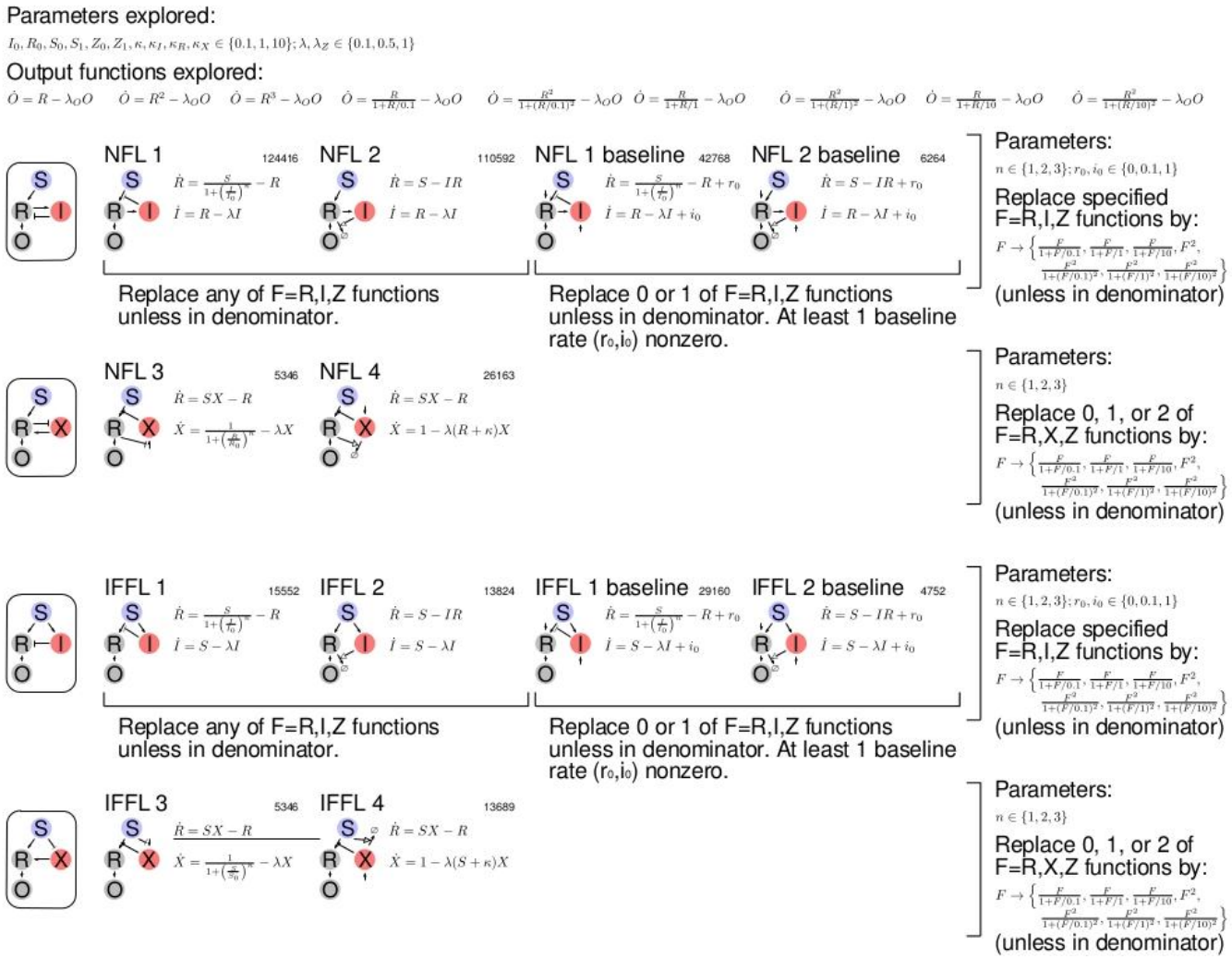

Supplementary Figure 2

Systematic enumeration of 3+1 NFL and 3+1 IFFL circuit topologies for computational analysis.

Each circuit topology is associated with a set of equations that are indicated. These models were further diversified by replacing I(t), R(t), X(t), Z(t) by other functional forms, e.g., I(t) → I(t)/(1 + I(t)/0.1), as specified. To keep the number of combinations computationally tractable, the number of replacements had to be limited as specified. The numbers next to the circuit names indicate the number of resulting combinations of parameters and functional forms that were evaluated.

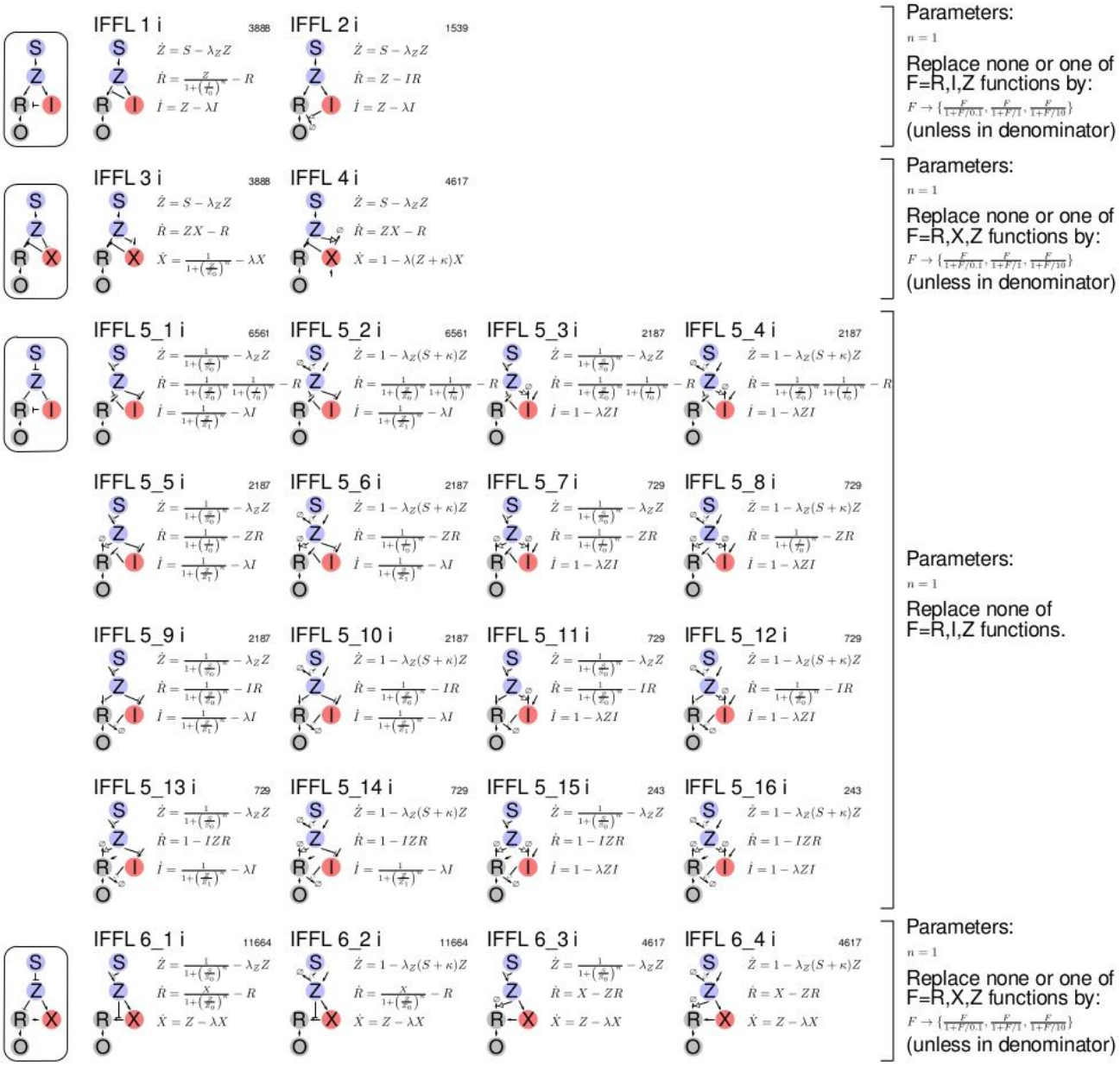

Supplementary Figure 3

Systematic enumeration of 4+1 IFFL circuit topologies with an intervening upstream node.

Also see Supplementary Figure 2.

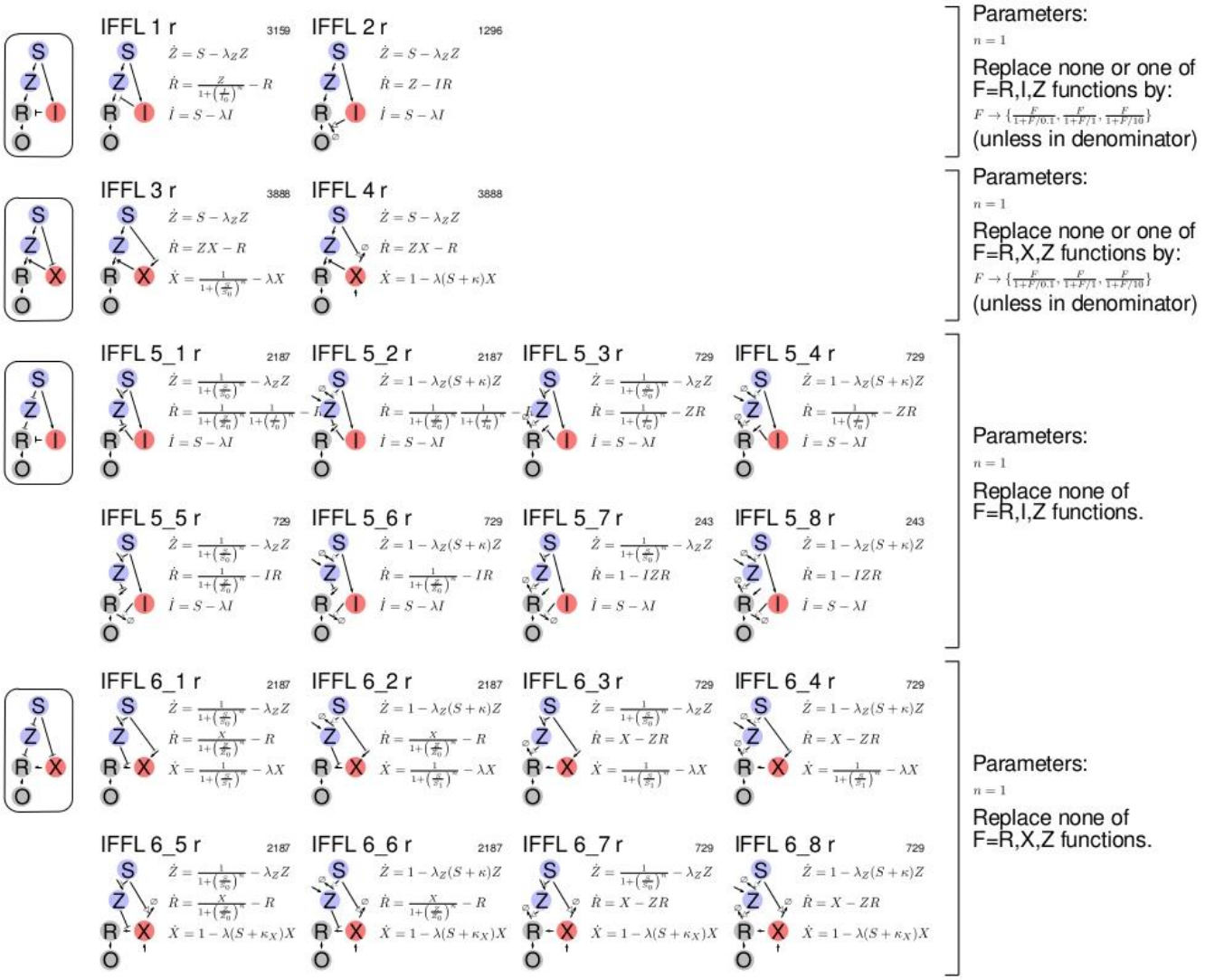

Supplementary Figure 4

Systematic enumeration of 4+1 IFFL circuit topologies with a node between the stimulus *S* and the response node *R*.

Also see Supplementary Figure 2.

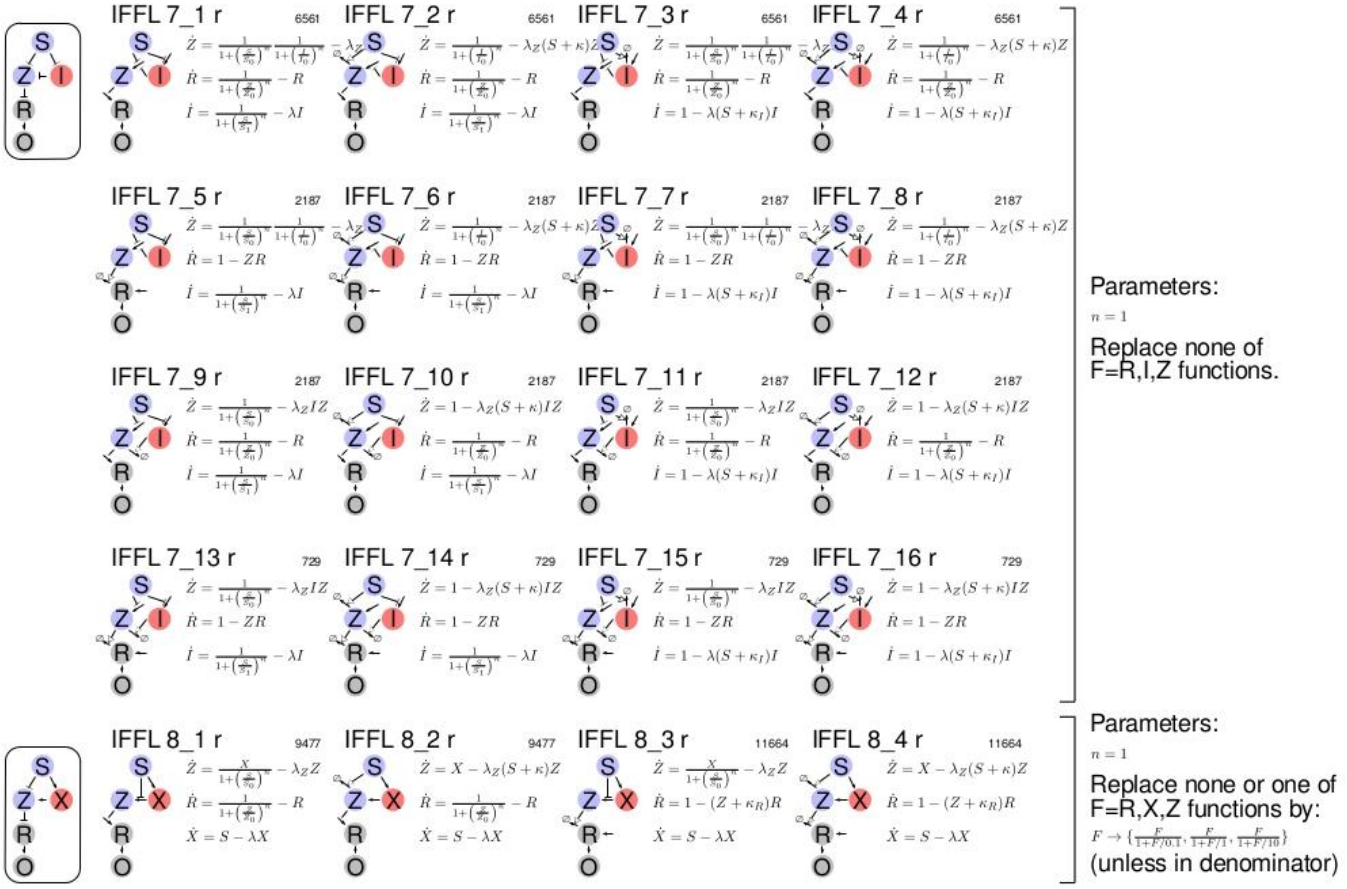

Supplementary Figure 5

Systematic enumeration of 4+1 IFFL circuit topologies with an adapting node *Z*, which is depressed by the stimulus and which in turn depresses the response node *R*.

Also see Supplementary Figure 2.

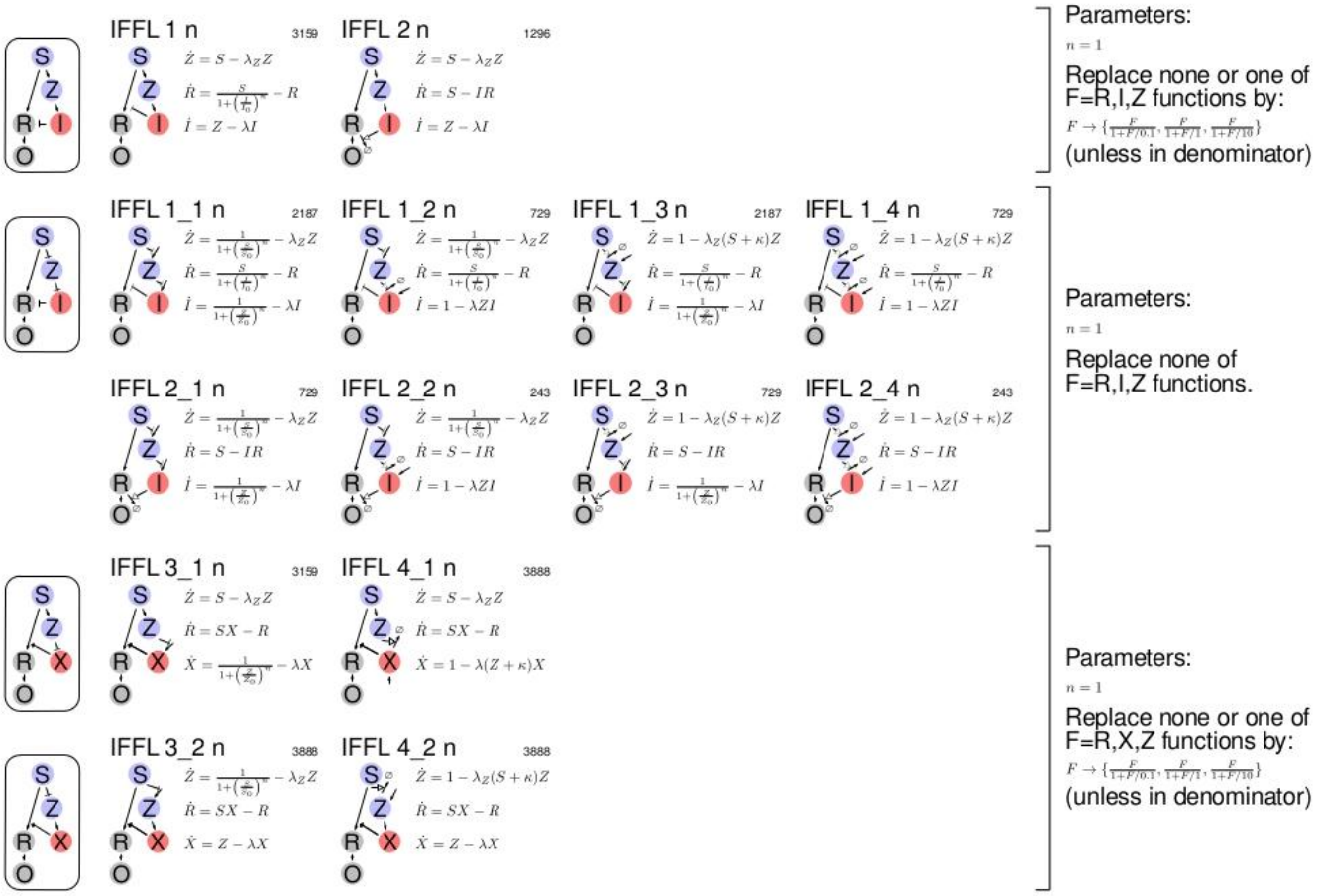

Supplementary Figure 6

Systematic enumeration of 4+1 IFFL circuit topologies with a node between the stimulus *S* and the inhibitory node *I* (or the activating node *X*).

Also see Supplementary Figure 2.

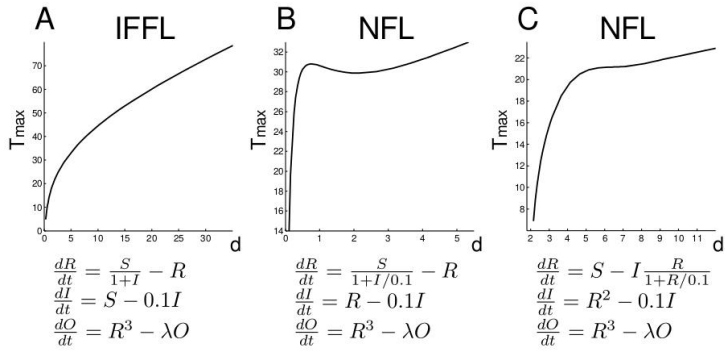

Supplementary Figure 7

Examples of $T_{max}(d)$ plots from the computational search.

Examples of T_{max}(d) plots from the computational search summarized in Table 1. A-C: λ is arbitrary. A: An IFFL model with simple (non-cooperative) Michaelis-Menten inhibition. B: An NFL model with simple (non-cooperative) Michaelis-Menten inhibition showing that T_{max}(d) can even have a negative slope. C: An NFL model in which the inhibitor I degrades the response R.

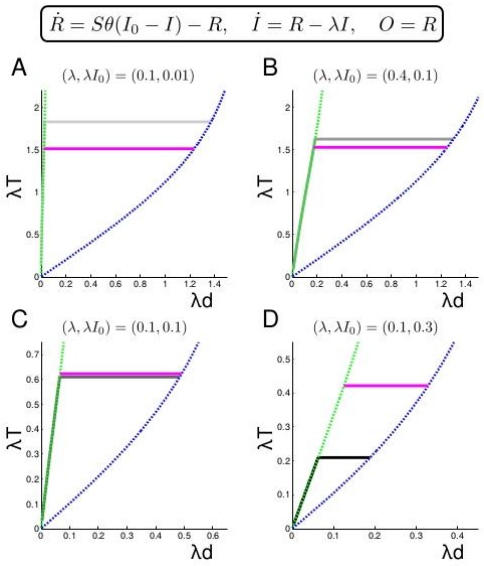

Supplementary Figure 8

Detailed analysis of NFL circuits.

Detailed analysis of NFL circuits in Fig. 1 F, J showing that $T_{max}(d)$ (grey lines) and pulse periods and widths leading to period skipping (magenta-green-blue triangles below magenta lines) are close for a variety of model parameters. Thus, a search for T_{max} may be expected to lead to observing period skipping as well, if it occurs. Grey lines: $T_{max}(d)$ plotted with the same shades of grey as in Fig. 1 J. Magenta lines: In the triangles between the green, blue, and magenta lines (below the magenta lines), periodic solutions with the same period T as the stimulus period are unstable and period skipping is observed. Blue dashed lines: The regions of interest for our analysis are to the left of the blue dashed lines in each panel; to the right of the blue dashed lines, each stimulus pulse is so long that the circuits respond at least twice to each stimulus pulse (R goes up at least twice), because each stimulus pulse extends beyond the time when the circuit recovers from adaptation, i.e., when I drops below I_0 again, and can be activated again. This may be a feature of these models that is not observed in many biological NFLs and thus we refrain from analyzing the models in this regime. Green dashed lines: To the left of the green dashed lines, the pulse durations d are too short (alternatively, the pulse periods T too long) for enough inhibitor I to accumulate during each periodic stimulus pulse to block the stimulus pulses at all and thus for the responses to show any adaptation; $\theta(I_0 - I)$ is always equal to 1. To the right of the green dashed lines, the pulse durations d are long enough (alternatively, the pulse periods T short enough) for enough inhibitor to accumulate during each stimulus pulse to block the stimulus pulses at some point after the onset of each stimulus pulse. For any fixed pulse period T, making the pulse durations d longer than specified at the green boundary has the same effect as stimulus pulses with pulse durations at the green boundary because the inhibitor cuts the stimulus off ($\theta(I_0 - I) = 0$) for pulse durations to the right of the boundary line.

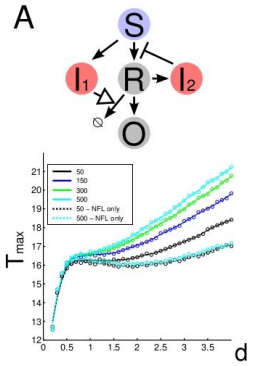

Supplementary Figure 9

Disentangling multiple circuit motifs.

A: $T_{max}(d)$ for a pathway combining an IFFL circuit (through I_1) with slower kinetics and an NFL circuit (through I_2) with faster kinetics, acting in parallel. After the onset of on-off pulsing, the NFL circuit influences the output quickly whereas the IFFL circuit affects the output more slowly. So, we measured the running average of the output (= O(d, T)) at different time points 50, 150, ... after the onset of the periodic on-off stimulus. For the NFL-only circuit (I_2 set to 0, dashed lines), which is presented for comparison, $T_{max}(d)$ is strongly stabilized and in fact decreases at intermediate d. In the full circuit, as O(d, T) is defined at later time points, T_{max} stabilization slowly disappears (black→blue→green→cyan). ($dI_1/dt = S - \lambda_1 I_1$, $dI_2/dt = R - \lambda_2 I_2$, $dR/dt = S/(1 + (I_2/I_0)^n) - (1 + \kappa I_1)R$, $O(t) = R^3(t)$, $\lambda_1 = 1/200$, $\lambda_2 = 2/10$, $\kappa = 1/100$, $n = 1$, $I_0 = 1/10$)

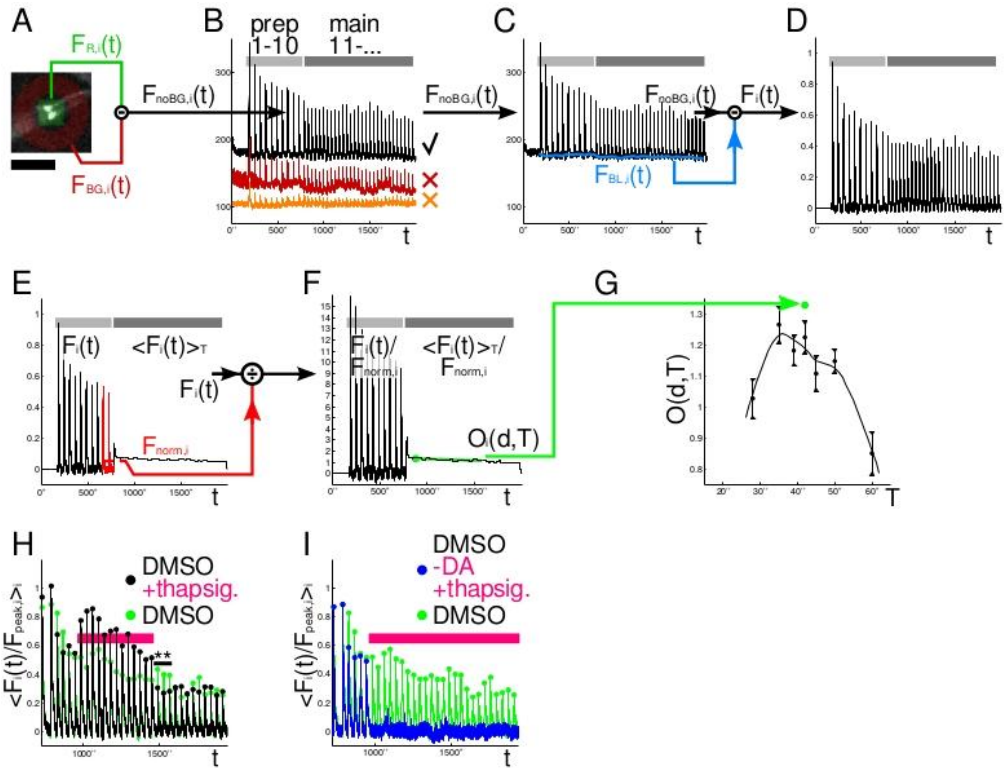

Supplementary Figure 10

Processing of *C. elegans* experimental data and additional pharmacological experiments.

For details, see Methods. In all experiments, the main odor pulses (here: d = 20'', T = 42'') were preceded by 10 preparatory odor pulses of duration 10'' and period 60''. A: One imaged frame (cropped, of about 20000 total frames per experiment, recorded at 10 Hz) showing GCaMP fluorescence from the AWA neuron pair of a single worm. $F_{R,i}(t)$ is the average intensity over the area indicated by a green square, centered on the AWA neurons, and $F_{BG,i}(t)$ is the median intensity over the region indicated by a red ring. Scale bar: 100µm. B: $F_{noBG,i}(t) = F_{R,i}(t) - F_{BG,i}(t)$ plotted for different worms from the same experiment. The red trace is filtered out because the baseline moves too much (6.5%) before and after the preparatory odor pulse 10. The orange trace is discarded because the noise-to-signal ratio (0.11-0.15) is too high. See Methods for more details. C: A piecewise linear function $F_{BL,i}(t)$ (blue) representing the time-dependent baseline fluorescence is fit through $F_{noBG,i}(t)$ before each response pulse. D: Plot of $F_i(t) = F_{noBG,i}(t)/F_{BL,i}(t)-1$, which is corrected for the baseline fluorescence $F_{BL,i}(t)$. E: $F_i(t)$ is plotted for the preparatory pulses and its running average over a time window of size T is plotted for the main pulses. The mean of $F_i(t)$ over the preparatory pulses 9 and 10 (= $F_{norm,i}$, area indicated in red divided by 120'') is shown as a horizontal red bar. F: $F_i(t)$ is normalized by $F_{norm,i}$; then, the normalized running average is fit to a straight line between 100''-800'' after the beginning of the main odor pulses. G: The value of the linear fit at 100'' after the beginning of the main odor pulses represents the output data point $O_i(d, T)$ for worm i at pulse duration d and period T. H, I: Fig. 3 I underlain for comparison. H: Same as Fig. 3 E except thapsigargin applied longer (for additional three odor pulse periods). Mean over 13 worms. I: Thapsigargin applied but odor stimulus pulses turned off. Thapsigargin presentation in the absence of odor only caused minor and brief increases in Ca^{2+}, potentially, by disrupting baseline Ca^{2+} maintenance. Mean over 14 worms.

Supplementary Note 1:
Advantages to oscillatory stimulation approach

Because of the way we defined $T_{\max}$, our results automatically extend to an infinite set of variations of each explicit circuit model we studied (Fig. 1 K). These variations do not change $T_{\max}$. Therefore, by analyzing representative models (Supplementary Figs. 2-6), we studied all related variants (Fig. 1 K): i) Each model is trivially equivalent to other models by rescaling the variables, which is why we studied $S = 0$ or $= 1$ only. ii) Nodes that merely delay signals anywhere along the signal transduction pathway do not change $T_{\max}$ as long as the final inputs U_m and U_n in Fig. 1 K are simultaneous. iii) Upstream nodes (from S to U_m and U_n in Fig. 1 K) that nonlinearly transform the input do not change the on-off stimulus except for rescaling. Therefore, our scheme is, in principle, robust to nonlinearities upstream of the adaptation mechanism. iv) Furthermore, repeated input pulses permit us to take advantage of a simple trick: The time average of the output $O(d, T)$ is directly proportional to the time average of further upstream elements in the signal transduction cascade, if the intervening nodes have first-order kinetics ($\dot{W}_i = k_{i,+}W_{i-1} - k_{i,-}W_i$ implies that $\langle W_i \rangle$ is proportional to $\langle W_{i-1} \rangle$). This means that we only needed to analyze explicitly circuits whose output passed through nonlinear filters (up to V_p in Fig. 1 K) and we could neglect further downstream nodes with first-order dynamics. Also, this means that in practice, the measured output does not need to be deconvolved mathematically to reconstruct the underlying responses as long as the intervening processes are first-order, for example, folding and maturation of reporter fluorescent proteins can be ignored[44]. v) Lastly, in each numerical calculation, we explicitly modeled the dynamics of $O(t)$ with Michaelis-Menten and Hill coefficients as a function of $R(t)$, for example, to represent GCaMP Ca^{2+} binding cooperativity[40]. The explicitly modeled nonlinearities could represent multiple successive output nonlinearities, e.g., $V_1 = R^2$ and $\dot{O} = V_1/(1 + V_1/V_0) - \lambda_O O$ (Fig. 1 K).

Other advantages to using periodic stimuli and measuring the average of the output are that transients and the dependence on initial conditions disappear in many dynamical systems with repeated pulsing[45]; the mathematical description and the analysis of the system simplify, for example, initial conditions become irrelevant. Also, the time average of the output is less susceptible to random measurement noise than any particular point in a recording, e.g., the height of a peak.

Supplementary Note 2: Mathematical proofs for no period skipping in IFFLs

Feedforward systems

We begin by considering purely feedforward systems (such as the IFFL in Fig. 1 E, I), where the dynamical elements $\{x_1, \ldots, x_n\}$ satisfy the property that if x_i influences x_j, then x_j does not influence x_i. This means that the network nodes can be arranged in a sequence $x_1 \to x_2 \to \ldots \to x_n$ (potentially by relabeling) such that no element influences another to its left. In such a dynamical system where $\dot{x}_i = f_i(\{x_1, \ldots, x_i\}, t)$, the Jacobian ($J_{ij} = \partial f_i / \partial x_j$) is lower triangular. We make the following assumptions, which are appropriate for biochemical systems: i) The diagonal elements of J are negative, specifically, the degradation rates have strictly positive lower bounds (i.e., $\partial f_i(\{x_1, \ldots, x_i\}, t)/\partial x_i \leq -c_i^2 < 0$), because every species is degraded in a concentration-dependent manner and the degradation rates do not vanish, at least, when the system is stimulated periodically. Linear degradation terms $\sim -k_i x_i$ and Michaelis-Menten terms $\sim -k_i x_i/(1 + x_i/x_{i0})$ (assuming x_i is bounded from above) fulfill this requirement, as well as Michaelis-Menten terms with Hill coefficients $\sim -k_i x_i^n/(1 + x_i^n/x_{i0}^n)$, where n reflects cooperativity $n > 1$ and x_i is bounded from below, e.g., due to the periodic stimulation. ii) The off-diagonal elements of J are bounded, i.e., all $|J_{ij}| < p_{\max}$.

Theorem 1: A feedforward system satisfying these two conditions has a unique periodic solution with period T (same as stimulus), to which every other solution converges. (For additional technical conditions, see Theorem 2 in ref.[45].)

Proof: By choosing a diagonal matrix P with $P_{ii} = 1/p^i$, we can make the off-diagonal elements of PJP^{-1} arbitrarily close to zero, the larger $p \gg p_{\max}$ is. Then, the matrix measures μ_1, μ_2, or μ_∞, associated with the L^1, L^2, or L^∞-norms, respectively, of PJP^{-1} are all approximately equal to the largest (i.e. least negative) diagonal element. Thus, the system is infinitesimally contracting with a positive contraction rate, and by theorem 2 in ref.[45], all $x_i(t)$ are T-periodic. □

Positive feedback loops

The previous theorem pertains to feedforward systems without any closed loops, i.e., no influence of downstream nodes on upstream nodes. This leaves open the possibility of period skipping in systems which contain positive feedback loops (PFLs) as well as IFFLs. Such PFLs would have to be entirely upstream or downstream of any IFFLs in the signal transduction cascade because a connection from the adapting node or its downstream nodes back upstream of the adapting node would create a NFL. So, we consider PFLs feeding into an IFFL feeding into another system of PFLs, and we wish to show that the composite system cannot show period skipping.

A few definitions and previous results are needed. By a system of PFLs ($\dot{\vec{x}}(t) = \vec{f}(\vec{x}(t), \vec{u}(t))$), we mean specifically that the two inequalities

$$\frac{\partial f_i}{\partial x_j}(\vec{x}, \vec{u}) \geq 0 \quad \forall i \neq j \quad \text{and} \quad \frac{\partial f_i}{\partial u_j}(\vec{x}, \vec{u}) \geq 0 \quad \forall i, j$$

hold for all $\vec{x}$ and stimuli $\vec{u}$. The former inequality implies that the elements in the system only influence each other positively, i.e., lead to each other's increase, and the latter condition that the stimulus $\vec{u}(t)$ influences the elements of the system only positively as well. Systems satisfying the former condition are 'cooperative'. Thus, by PFLs we not only mean that the dynamic nodes increase each other but also that the input, e.g., the applied external stimulus, only increases the nodes that it influences directly.

Such systems are 'monotone'[46]:

$$\vec{x}^{(1)}(t_0) \geq \vec{x}^{(2)}(t_0), \vec{u}^{(1)}(t) \geq \vec{u}^{(2)}(t) \quad \forall t \geq t_0 \quad \text{implies} \quad \vec{x}^{(1)}(t) \geq \vec{x}^{(2)}(t) \quad \forall t \geq t_0 \quad . \tag{1}$$

(For simplicity, we abbreviate the component-wise inequality $x_i \geq y_i$ for all vector components i by $\vec{x} \geq \vec{y}$.) Monotonicity is a more general condition on dynamics; here, we study the special cases of cooperative systems (with inputs).

An important result for periodically forced monotone systems $\dot{\vec{x}} = \vec{f}(\vec{x}(t), \vec{u}(t))$ is given as Theorem 5.26 in [Hirsch2005], which credits the unpublished 1997 Ph.D. thesis by I. Tereščák. This result applies to systems that are irreducible, meaning that all its Jacobian matrices are irreducible (i.e., every variable can indirectly affect every other variable, possibly through an arbitrary number of intermediates; see also

[Hirsch 2003]). The result states that $\vec{x}(t)$ converges to a solution with period kT, where $k \geq 1$ is an integer, for almost all initial conditions if the stimulus $\vec{u}(t)$ is periodic with period T ($\vec{u}(t) = \vec{u}(t+T)$). It is important to note that, generally, there may be stable periodic solutions with period kT and $k > 1$, as shown in [Takac 1992]. Thus, we present additional conditions, appropriate for biological systems, which insure that $k = 1$. Since the set of initial conditions which lead to non-kT-periodic solutions has measure zero, we consider those cases negligible for our purposes.

2D positive feedback loops

First, we show that a PFL, which only contains two dynamical elements and which is stimulated with period T, if it has a solution with period kT, where k is an integer, then k equals 1; thus, period skipping with $k = 2, 3, \ldots$ is not possible. A related result exists in the literature: All 2D periodic irreducible cooperative systems approach a T-periodic solution [Hale 1983], which excludes chaotic solutions and noninteger k as well. Regardless, we present the following lemma and corollary because the proofs are self-contained and build towards the results in the subsequent section, and also because we do not need to assume irreducibility:

Lemma 1: Consider a 2D dynamical system, driven by an input of period T, ($\dot{\vec{x}}(t) = \vec{f}(\vec{x}(t), \vec{u}(t))$ where $\vec{x}(t) \in \mathbb{R}^2_+$ and $\vec{u}(t) = \vec{u}(t+T)$), and suppose that $\vec{x}(t_0)$ is a periodic point with some period kT, where k is a positive integer. Then there is some time t_1 so that $\vec{x}(t_1) \leq \vec{x}(t_1 + T)$ or some time t_2 so that $\vec{x}(t_2) \geq \vec{x}(t_2 + T)$.

Proof: Suppose without loss of generality that $t_0 = 0$ and that (otherwise we are done, with $t_1 = 0$) $x_1(0) > x_1(T)$ and $x_2(0) < x_2(T)$ (if the opposite inequalities hold, the argument is analogous). There is some integer $s > 1$ so that $x_1((s-1)T) \leq x_1(sT)$ since, otherwise, $x_1((s-1)T) > x_1(sT)$ for all s, and therefore $x_1(0) = x_1(kT) < x_1((k-1)T) < \ldots < x_1(0)$, which is a contradiction.

Now pick any such s and let $S = (s-1)T$. Then, the continuous function $p(t) := x_1(t) - x_1(t+T)$ has $p(0) > 0$ and $p(S) \leq 0$, so there is some minimal t_1 so that $p(t_1) = 0$.

Similarly, consider $q(t) := x_2(t) - x_2(t+T)$, which has $q(0) < 0$, and conclude that there is some minimal t_2 so that $q(t_2) = 0$. Suppose that $\min\{t_1, t_2\} = t_1$. Then $x_1(t_1) = x_1(t_1 + T)$ and $x_2(t_1) \leq x_2(t_1 + T)$. If instead $\min\{t_1, t_2\} = t_2$, then the other inequality holds. □

Before proving the following corollary, we introduce the notation $F(\vec{x}(s)) = \vec{x}(s+T)$ for the solution to

the differential equation $\dot{\vec{x}}(t) = \vec{f}(\vec{x}(t), \vec{u}(t))$ at time $s+T$ starting with initial condition $\vec{x}(s)$ at time s. Furthermore, we denote by $F^k(\vec{x}(s)) = \underbrace{F \circ \ldots \circ F(\vec{x}(s))}_{k \text{ times}}$ the k-fold mapping of the initial condition $\vec{x}(s)$. Note that $F^k(\vec{x}(s)) = \vec{x}(s+kT)$, which we prove by induction: For $k=1$, it follows from the definition. Next, assuming that $F^n(\vec{x}(s)) = \vec{x}(s+nT)$ holds, we define $\vec{z}(t) = \vec{x}(t+nT)$ and note that $\dot{\vec{z}}(t) = \dot{\vec{x}}(t+nT) = \vec{f}(\vec{x}(t+nT), \vec{u}(t+nT)) = \vec{f}(\vec{z}(t), \vec{u}(t))$, where the last equality follows from the definition of $\vec{z}$ and the periodicity of $\vec{u}$. So, like $\vec{x}(s)$ before, we can map $\vec{z}(s)$ forward in time by one period $\vec{z}(s+T) = F(\vec{z}(s)) = F(F^n(\vec{x}(s))) = F^{n+1}(\vec{x}(s))$, and, also, $\vec{z}(s+T) = \vec{x}(s+nT+T) = \vec{x}(s+(n+1)T)$. Thus, we have $F^{n+1}(\vec{x}(s)) = \vec{x}(s+(n+1)T)$. □

Using this notation and the monotonicity property, we prove the following:

Corollary: Suppose the system is monotone, in addition to the conditions in Lemma 1, and $\vec{x}(t)$ is periodic with period kT ($\vec{x}(t) = \vec{x}(t+kT)$), then $\vec{x}(t+T) = \vec{x}(t)$ for all t, i.e., the orbit of $\vec{x}$ has period T.

Proof: The mapping F is monotone by assumption (Eq. (1)). We pick the time t_1 as in Lemma 1 (the proof would be analogous with t_2), so $\vec{x}(t_1) \leq F(\vec{x}(t_1)$. By monotonicity, the inequality is preserved under repeated mappings, $F^n(\vec{x}(t_1)) \leq F^{n+1}(\vec{x}(t_1))$. So, iterating, $\vec{x}(t_1) \leq \vec{x}(t_1+T) \leq \vec{x}(t_1+2T) \ldots \leq \vec{x}(t+kT) = \vec{x}(t)$, where the last equality comes from the assumption that $\vec{x}(t)$ has period kT. Since $\vec{x}(t_1) = \vec{x}(t_1+T)$, we have $\vec{x}(t) = \vec{x}(t+T)$ for all times t. □

Positive feedback loops stimulated from rest

Next, we consider systems of PFLs $\dot{\vec{x}}(t) = \vec{f}(\vec{x}(t), \vec{u}(t))$ with $\vec{x}(t)$ consisting of any finite number of components, i.e., not restricted to two as in the previous section. We show that period skipping trajectories are inaccessible to the system if it is initially at rest before periodic stimulation, even if the PFL system could exhibit period skipping in principle.

First, we note that a non-negative stimulus always raises the concentrations of the components of a PFL system relative to the steady state where the stimulus is off: From the monotonicity property in Eq. (1), we have that $\vec{x}^{(1)}(t) \leq \vec{x}^{(2)}(t)$ for all $t \geq 0$ if the systems starts from the same initial state $\vec{x}(0)$ and if the inputs satisfy $\vec{u}^{(1)}(t) \leq \vec{u}^{(2)}(t)$ for all $t \geq 0$. So, if we compare the steady state (i.e. with input $\vec{u}^{(1)}(t) = 0$) to the system after the onset of stimulation, i.e., $\vec{u}^{(2)}(t)$ is non-negative for all $t \geq 0$, and $\vec{x}(0) = x_{\text{ss}}$ is the steady state, it follows that $\vec{x}_{\text{ss}} = \vec{x}^{(1)}(t) \leq \vec{x}^{(2)}(t)$ for all $t \geq 0$.

In the following, we imagine that $\vec{x}$ is the state of the system after sufficiently many stimulus pulses,

starting from $\vec{x}_{\rm ss}$ initially, such that the solution has converged to a kT-periodic solution (and we show that $k = 1$):

Theorem 2: Let F (introduced in the previous section) be a monotone mapping. Suppose that these properties hold for two fixed states $\vec{x}$ and $\vec{x}_{\rm ss}$:

(1) $\vec{x}_{\rm ss} \leq F(\vec{x})$

(2) $F^k(\vec{x}) = \vec{x}$ for some integer $k \geq 1$

(3) $F^l(\vec{x}_{\rm ss}) - F^l(\vec{x}) \to 0$ as $l \to \infty$

Then $F(\vec{x}) = \vec{x}$.

Proof: Pick an integer $n \geq 0$. Then, for any integer $r \geq 1$:

$$F^n(\vec{x}) = F^{rk+n}(\vec{x}) = F^{rk+n}(\vec{x}) - F^{rk+n}(\vec{x}_{\rm ss}) + F^{rk+n}(\vec{x}_{\rm ss}) \leq q_r + F^{rk+n+1}(\vec{x}) = q_r + F^{n+1}(\vec{x})$$

where $q_r = F^{rk+n}(\vec{x}) - F^{rk+n}(\vec{x}_{\rm ss})$ and where we used (2) to obtain $F^n(\vec{x}) = F^{rk+n}(\vec{x})$, then (1) to get $F^{rk+n}(\vec{x}_{\rm ss}) \leq F^{rk+n}(F(\vec{x})) = F^{rk+n+1}(\vec{x})$ and finally again (2) to get $F^{rk+n+1}(\vec{x}) = F^{n+1}(\vec{x})$. Using (3), $q_r \to 0$ as $r \to \infty$, so we conclude that $F^n(\vec{x}) \leq F^{n+1}(\vec{x})$ for all $n \geq 0$.

Thus,

$$\vec{x} \leq F(\vec{x}) \leq F^2(\vec{x}) \leq \ldots \leq F^k(\vec{x}) = \vec{x} \quad ,$$

and therefore $F(\vec{x}) = \vec{x}$. □

Theorem 2 ensures that, if a system is monotone and the input is periodic with period T, then the solution when starting from a steady-state cannot approach a periodic orbit of (minimal) period kT, where $k > 1$ is an integer.

Composite PFL → IFFL → PFL systems

Stitching together our mathematical results for purely feedforward systems and PFLs, we see that period skipping is impossible in a composite $S \to$ PFL $\to$ IFFL $\to$ PFL sytem, where $S(t)$ is the applied periodic on-off stimulus ($= \vec{u}(t)$ in the above proofs for the first PFL in the signaling cascade). This leaves period skipping generically to NFLs. There are, however, two subtleties:

In the first step of the cascade ($S \to$ PFL) the above proofs apply exactly but in the subsequent steps (PFL $\to$ IFFL and IFFL $\to$ PFL), the input is no longer exactly periodic but converges to a periodic

function of time. While this may be a concern in general, here it is not: i) For a contractive system such as the purely feedforward system described above, if the stimulus approaches the periodic stimulus $\vec{u}(t)$, the solution approaches the periodic solution $\vec{x}(t)$ for stimulus $\vec{u}(t)$. This follows from the main results in [Desoer 1972] and more generally the theory developed in [Aminzare 2014]. Thus, for the PFL $\rightarrow$ IFFL step, our previous result of no-skipping in purely feedforward systems continues to hold. ii) Similarly, for monotone systems such as the PFLs, the solution approaches the solution $\vec{x}(t)$ for the periodic stimulus $\vec{u}(t)$ if the stimulus approaches $\vec{u}(t)$. This property is the analogue, for stable periodic orbits instead of stable steady states, of the "convergent input convergent state property" for monotone systems which was treated in ref.[46]. We omit the proof, which is similar. Thus, for the IFFL $\rightarrow$ PFL step, our result of no-skipping in 2D or no-access to skipping in general PFL systems continues to hold as well.

Another issue is that in our definition of PFLs, we assumed that the stimulus only influences the nodes of the PFL positively. While this is a straightforward assumption for the first step in the cascade ($S \rightarrow$ PFL), it also has to hold for the way the IFFL feeds the final PFL (IFFL $\rightarrow$ PFL). If it does not hold, the system may contain additional adapting circuits and a further break-down into subcircuits is necessary for the analysis.

Supplementary References

[Aminzare 2014] Aminzare, Z. & Sontag, E. Contraction methods for nonlinear systems: A brief introduction and some open problems. In: Proc. IEEE Conf. Decision and Control, Los Angeles, Dec. 2014, 3835–3847 (2014).

[Desoer 1972] Desoer, C. & Haneda, H. The measure of a matrix as a tool to analyze computer algorithms for circuit analysis. IEEE T. Circuits. Syst. 19, 480–486 (1972).

[Hale 1983] Hale, J. K. & Somolinos, A. S. Competition for fluctuating nutrient. J. Math. Biology 18, 255–280 (1983).

[Hirsch 2003] Hirsch, M. W. & Smith, H. L. Competitive and Cooperative Systems: A Mini-review, In: Positive Systems: Proceedings of the First Multidisciplinary International Symposium on Positive Systems: Theory and Applications (POSTA 2003), 183–190 (Springer Berlin Heidelberg, 2003).

[Hirsch 2005] Hirsch, M. W. & Smith, H. Monotone dynamical systems, In: Handbook of differential equations: ordinary differential equations. Vol. II, 239–357 (Elsevier B. V. Amsterdam, 2005).

[Takac 1992] Takáč, P. Linearly stable subharmonic orbits in strongly monotone time-periodic dynamical systems. Proc. Amer. Math. Soc. 115, 691–698 (1992).

Supplementary Note 3: Published models

To decide whether any individual adaptation mechanism is an IFFL or NFL, one has to examine whether the adaptation mechanism is direct (independent of the response R) (IFFL) or indirect (dependent on the response R) (NFL).

State-dependent inactivation model

The dynamical system in ref.[9],

$$\dot{x} = \alpha(u(t))(A - x) - \beta(u(t))x - \gamma x + \Delta$$
$$\dot{A} = -\gamma x + \Delta,$$

where x is the active species and A the sum of the active species x and the inactive species $y(= A - x)$, can be rewritten in terms of x and y,

$$\dot{x} = \alpha(u(t))y - \beta(u(t))x - \gamma x + \Delta$$
$$\dot{y} = \beta(u(t))x - \alpha(u(t))y.$$

This transformation just re-expresses the central reactions in the Friedlander-Brenner scheme,

$$y \underset{\beta(u(t))}{\overset{\alpha(u(t))}{\rightleftharpoons}} x \underset{\Delta}{\overset{\gamma}{\rightleftharpoons}} \text{unavailable} \quad ,$$

in terms of x and y instead of x and the sum $A = x + y$.

For perfect adaptation, Δ is chosen to be constant, as in Fig. 2 E-F in ref.[9]. There is clearly no NFL in the system, since x and y influence each other positively (assuming that $\alpha(u(t)), \beta(u(t)) > 0$, as in ref.[9]). The circuit adapts because $\alpha(u(t))$ turns on x directly (in a y-dependent manner), but reduces y directly (independently of x) as well, leading to the subsequent decay of x. This is clearly an IFFL, and it is the same basic mechanism as in the IFFL circuit B in Fig. 1 or IFFL 4 in Supplementary Fig. 2 with $x \to R$ and $y \to X$ roughly analogous. This may be a difficult case for recognizing the IFFL topology

because the depletion of y and build-up of x are linked molecularly in the same process, but that does not change the basic mechanism of the IFFL circuit, in which $\alpha(u(t))$ builds up x and depletes y directly (independently of x), the latter being responsible for adaptation. Of course, our IFFL models do not have the additional features of the Friedlander-Brenner model such as a positive feedback loop.

We used the model and parameters in Fig. 2 E-F of ref.[9] to verify that this model neither shows periodic skipping nor refractory period stabilization, as expected for an IFFL. To observe the refractory period, we chose as output nonlinearities $O(d,T) = \langle x^2 \rangle$ or $O(d,T) = \langle x^3 \rangle$.

In ref.[10], the state-dependent inactivation model was presented in a simpler form:

$$\dot{A}_{\text{on}} = k_1 Input\,(1 - A_{\text{on}} - A_{\text{in}}) - k_2 A_{\text{on}}$$
$$\dot{A}_{\text{in}} = k_2 A_{\text{on}},$$

where the input converts protein $A_{\text{off}} = (1 - A_{\text{on}} - A_{\text{in}})$ into the 'on' form of the protein A_{on}, which is slowly converted into the inactive form A_{in}. This system adapts perfectly to a step input. To analyze the system further, we rewrite the equations in terms of A_{on} and A_{off} instead of A_{on} and A_{in}:

$$\dot{A}_{\text{on}} = k_1 Input A_{\text{off}} - k_2 A_{\text{on}}$$
$$\dot{A}_{\text{off}} = -k_1 Input A_{\text{off}}.$$

Both sets of equations of course describe the same reactions, only the transformed (latter) set describes the dynamics of A_{on} and A_{off}, which are central to the adaptation mechanism:

$$A_{\text{off}} \xrightarrow{Input*k_1} A_{\text{on}} \xrightarrow{k_2} A_{\text{in}} \quad .$$

As in the above case of the Friedlander-Brenner model, this system can be identified as an IFFL because the input increases A_{on} directly and at the same time decreases A_{off} directly (independently of A_{on}), which thus decreases A_{on} again, leading to adaptation. This too may be a difficult case for recognizing the IFFL topology because the depletion of A_{off} and build-up of A_{on} are linked molecularly in the same process, but that does not change the basic mechanism of the IFFL circuit, in which the $Input$ builds up A_{on} and depletes A_{off} directly (independently of A_{on}), the latter being responsible for adaptation.

Using the parameters in ref.[10] ($k_1 = 1$ and $k_2 = 1$), a constant influx into A_{off} to allow recovery ($\dot{A}_{\text{off}} = 1 - k_1 Input A_{\text{off}}$), an input that jumps from 0.01 (off) to 1 (on), and a nonlinearity $O(d,T) = \langle A_{\text{on}}^3 \rangle$ to observe a refractory period, we could not detect refractory period stabilization or period skipping in this system either, as in the above Friedlander-Brenner model and as expected for an IFFL.

We also note here for comparison that a simple phosphorylation/dephosphorylation system,

$$a \underset{k}{\overset{Input}{\rightleftharpoons}} b \quad ,$$

technically an IFFL, does not produce adaptation. Modifications such as the introduction of a third species as in the Friedlander-Brenner model are necessary to make this an adapting system.

Fold-change detection models

We used the models in Fig. 1 B, C in ref.[26], rewritten in terms of dimensionless parameters as in Eqns. (5) and (6) of ref.[26] with model parameters $T = 1$ and $T = 10$ for the IFFL model and the NFL model, respectively, as in Figs. 3 and 4 of ref.[26]. We found period skipping for the NFL model with pulse width $d = 0.2$ and pulse period 5, but neither period skipping nor refractory period stabilization in the IFFL model. We also switched the parameters (model parameter $T = 1$ for the NFL model or model parameter $T = 10$ for the IFFL model) and found the same results. Since an off stimulus $S = 0$ is difficult to implement computationally with these models, we chose $S = 0.001$ as our off stimulus (and $S = 1$ as usual for the on stimuli). To observe the refractory period, we chose as an output nonlinearity $O(d,T) = \langle y^2 \rangle$.

Supplementary Tables

circuit type	total # tested	# adapting	# skipping + # refrac. period stabilization
NFL	1152	391	279 (71%)
IFFL	1152	382	0 (0%)

Table S1:

Refractory period stabilization and period skipping in NFLs do not require step thresholds. We took the models in Fig. 1 E, F (same as I, J) and replaced $\theta(I_0 - I)$, which shuts off the stimulus S when the inhibitor $I(t)$ exceeds the threshold I_0 in an all-or-nothing fashion, by $1/(1+(I/I_0)^n)$ where $n \in \{1, 2, 3, 4\}$ and $I_0 \in \{0.01, 0.1, 1, 10\}$ as well as the output function $O = R$ by $\dot{O} = R^m/(1 + (R/R_0)^m) - \lambda_O O$ where $m \in \{1, 2\}$ and $R_0 \in \{0.1, 1, 10, \infty\}$ or $m = 3$ and $R_0 = \infty$. λ_O is irrelevant for $T_{\max}$. We varied $\lambda \in \{0.01, 0.02, 0.03, 0.1, 0.2, 0.3, 1.0, 10\}$. Overall, we varied parameters over 3 orders of magnitude, and read out 9 different variations of the output function. For details, see Methods.

Nature Methods: doi:10.1038/nmeth.4408